A Double-Sided Planar Transmission Medium Design for Ultra-Low Loss Planar Orthomode Transducers

by

Duncan Alexander Findlay

A Thesis Presented in Partial Fulfillment
of the Requirements for the Degree
Master of Science

Approved April 2019 by the
Graduate Supervisory Committee:

James Aberle, Chair
Constantine Balanis
Georgios Trichopoulos

ARIZONA STATE UNIVERSITY

May 2019

ABSTRACT

Microwave circuits are an essential part of technology in the modern day. Everything from cell phone communications, television and radio reception, medical imaging, and radar surveillance depend on microwave circuitry. Constant efforts are being made to introduce new methods of implementing more efficient microwave circuitry while maintaining well known fabrication methods. These improvements typically focus on lower loss, smaller size, and higher operating frequencies [1-6]. This thesis will focus on the specific application of a planar orthomode transducer (OMT) in Home Direct Broadcast (DBS) Systems used in residential satellite receivers. The need for low-loss circuitry becomes increasingly important in the realm of satellite reception, as the carrier to noise levels at the receiver can be as low as 10dB [7]. Interference and loss of signal integrity can occur very easily if the receiving network is not properly designed.

This thesis will investigate the design of a planar transmission media that produces ultra-low losses when compared to more conventional planar transmission media. This design, which is called Double Sided Suspended Stripline (DSSL), utilizes air as its primary propagation medium. The design will be similar to standard suspended stripline in geometry, but has signal traces on the top and bottom of the substrate. The traces are connected using plated through-hole vias. This geometry is hugely beneficial because it virtually eliminates one of the major loss mechanisms in classical microwave structures: dielectric loss. This thesis will focus mainly on empirically derived equations and performance metrics obtained through rigorous simulation.

A Alessandra, por todo su amor y apoyo

ACKNOWLEDGMENTS

I would like to thank Dr. James Aberle for his infinite patience and guidance throughout my graduate research. I would also like to thank ATCi for sponsoring the project. Thank you to my coworkers, Brian Daniel and Alex Nersesian, for taking the time to help me in my understanding of physics and engineering, and maintaining flexibility with me during my busy school semesters.

TABLE OF CONTENTS

Page

LIST OF TABLES……..vi

LIST OF FIGURES……...vii

CHAPTER

1 INTRODUCTION 1

Theory and Loss Mechanisms of Transmission Media..... 1

Comparing Different Transmission Designs..... 3

Literature Review..... 7

2 BACKGROUND FOR THE RESEARCH 9

Antenna Technology Communications Incorporated (ATCi)..... 9

3 STRUCTURE MODELING AND SIMULATION 15

Materials..... 15

Geometry..... 16

Transmission Line Simulation 17

Rat-Race Hybrid Simulation..... 22

Probe Optimization 30

High Frequency Performance 37

CHAPTER Page

SMA - Microstrip - DSSL Transition 39

4 CONCLUSIONS AND FUTURE WORK 44

Design Process 44

Future Work 45

REFERENCES……..45

LIST OF TABLES

Table Page

1 – Values of Relative Permittivity and Loss Tangent for Different Materials [13-14]... 15

2 – Design Examples Used to Derive Optimal Width Equation..... 19

LIST OF FIGURES

Figure Page

1. Dielectric vs Conductor Loss (Assuming Copper Conductor, Neglecting Surface Roughness) [9] 2

2. Field Lines in Standard Stripline with Rogers Duroid 5880 Substrate 3

3. Standard Suspended Stripline Design with Rogers RO 4003C Substrate 4

4. Double Sided Suspended Stripline with Rogers RO 4003C Substrate 4

5. Reflection Coefficients 5

6. Transmission Coefficients 6

7. Cross Polarized Channels Transmitted at the Same Frequency 10

8. Channels After Separation and Down-conversion 10

9. Simulsat 11

10. Receiving Network 12

11. Block Diagram of the Low Noise Block 12

12. Mechanical Structure of the Feed Network 13

13. Top View of the Planar OMT 13

14. Circular Waveguide Vertical and Horizontal Modes 14

15. Representative Cross-sectional View of the DSSL Design 16

16. ADS Stack-up with Conductor and Via Layers 17

17. Top View of the Transmission Line in ADS Momentum with Conductor and Via Layers 18

18. Simulation with Different Air-gap Spacing 18

Figure Page

19. Optimal Widths for Design Examples (Simulated vs Calculated) 19

20. S(1,1) and S(2,1) for Optimal Width 20

21. DSSL Model in Ansys HFSS 21

22. S(2,1) from HFSS 21

23. S(1,1) from HFSS 22

24. Ideal Rat-race S-matrix 23

25. Rat-race Hybrid in ADS Momentum 23

26. S(1,1) and S(2,1) for Optimal Width of a 70.7Ω line 24

27. Phase Difference Between Ports 1 and 4 of a Ratrace Hybrid 25

28. Equal Power Split Between Ports 1 and 4 25

29. Rat-race Model in HFSS 27

30. Port 4 (0 Degree Incident Phase) 27

31. Port 1 (180 Degree Incident Phase) 28

32. Phase Difference at Port 2 28

33. Power Split 29

34. Reflections at Each Port 29

35. Optimization Set-up in HFSS 30

36. HFSS Model of the C-band Horn Feed with Single and Differential Probes 31

37. Top View of the Single and Differential Probes 31

38. DSSL S(1,1) for Differential Probes 32

39. Comparison of the Differential Probe Response Between SSL and DSSL 32

40. DSSL S(1,1) for Single Ended Probe 33

Figure Page

41. Comparison of the Single-Ended Probe Response Between SSL and DSSL 33

42. HFSS Model for WR229 Waveguide Transitions 34

43. Side View of WR229 Waveguide HFSS Model 35

44. DSSL S(1,1) for Waveguide Probe Transitions 35

45. Comparison of the WR229 Waveguide Probe Response Between SSL and DSSL ... 36

46. HFSS Mesh for DSSL 37

47. Transmission Response for DSSL and SSL from 1GHz-40GHz 38

48. SMA Model in HFSS 40

49. SMA to MLIN to DSSL Transition in HFSS 41

50. Bottom View of the Transition with Ground Spacing Between MLIN and DSSL 41

51. Transition Response with and without SMA Connected 42

52. Dimensions for DSSL 45

1 INTRODUCTION

Theory and Loss Mechanisms of Transmission Media

Some of the most common types of planar transmission media include microstrip line (MSL) and standard stripline (SSL). These designs have well known empirical design equations and many software packages such as Keysight ADS have integrated design tools that make creating microstrip and stripline structures almost trivial. Other more niche designs, like suspended stripline (SSSL) or coplanar waveguide (CPW), also have well known properties and design equations that can be utilized for specific applications. Each transmission media has its own merits and its own limitations, and the focus of this thesis is the double sided stripline design that focuses primarily on low-loss, high sensitivity applications.

The main loss factors in these applications are conductor losses and dielectric losses, with dielectric losses being the dominant loss mechanism at high frequencies. The dielectric loss increases proportional to frequency, while conductor loss increases proportional to the *square root* of frequency.

$$\alpha_d \Rightarrow f \qquad \text{Dielectric Loss}$$

$$\alpha_c \Rightarrow \sqrt{f} \qquad \text{Conductor Loss}$$

While the dielectric and conductor loss equations depend on the geometry of the transmission media, they still exhibit the same relationship to frequency as described

above [8]. Figure 1 shows this relationship: conductor and dielectric loss versus frequency.

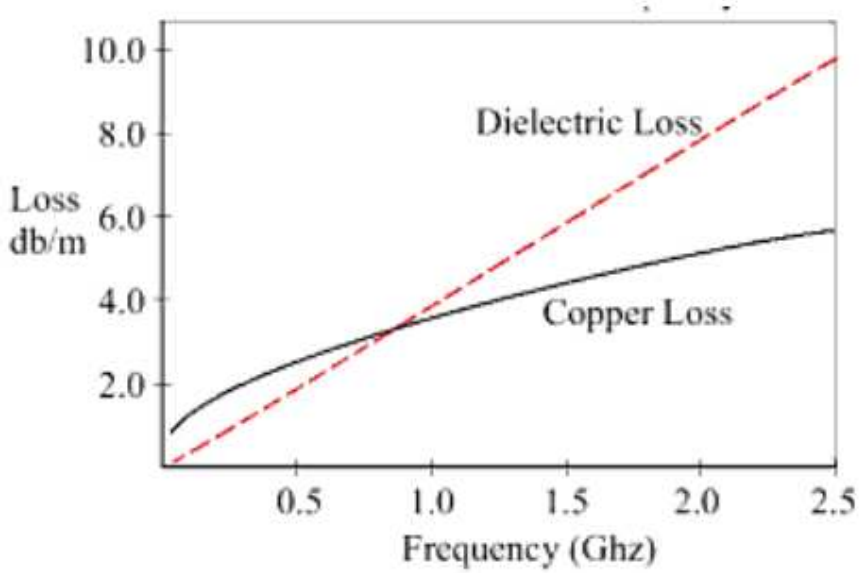

Figure 1 – Dielectric vs Conductor Loss (Assuming Copper Conductor, Neglecting Surface Roughness) [9]

We've made a case that dielectric losses are the major loss mechanism in transmission media at microwave frequencies, so by creating a new design that eliminates a large portion of this loss we can effectively improve the efficiency of our design. For applications that require minimal losses and maximum sensitivity, dielectric losses can be detrimental to the versatility and effectiveness of the design. Engineers often times must choose extremely expensive and high performing dielectric materials to prevent the dielectric loss from completely degrading signal integrity. This thesis will attempt to use cheaper and lower performing materials with a new design geometry that can outperform low loss and high cost materials utilized in conventional transmission media.

Comparing Different Transmission Designs

The following figures have been obtained using Ansys HFSS and help understand how the electric field lines behave in different transmission media.

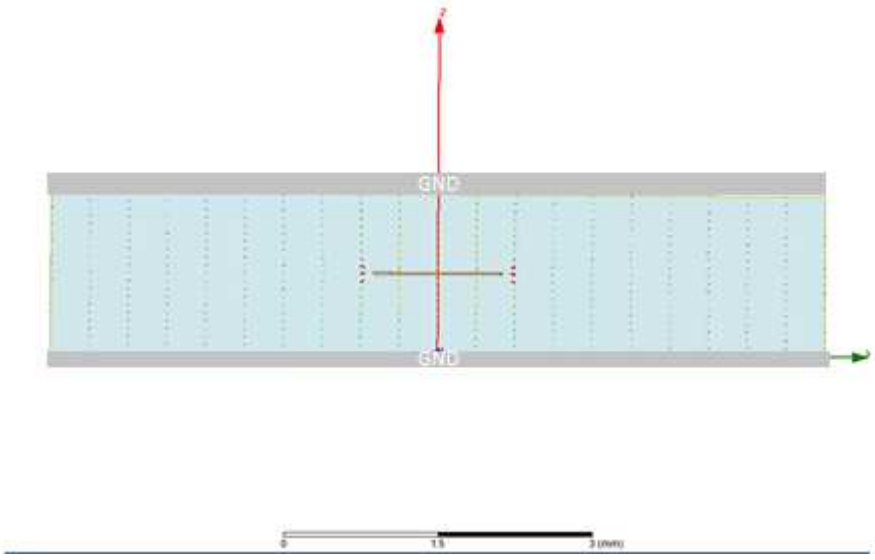

Figure 2 – Field Lines in Standard Stripline with Rogers Duroid 5880 Substrate

In Figure 2, we can see the field lines in a cross section of a standard stripline design. The field lines are entirely contained within the dielectric and will experience large dielectric loss.

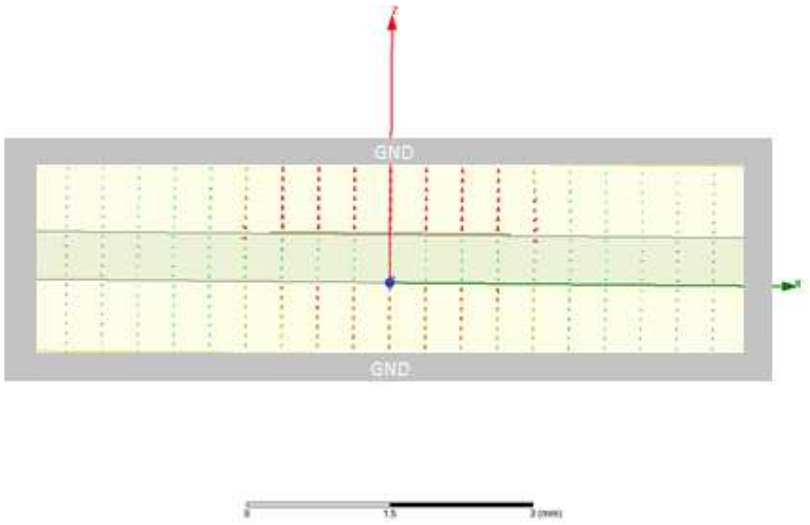

Figure 3 – Standard Suspended Stripline Design with Rogers RO 4003C Substrate

Figure 3 shows a cross-sectional view of a standard suspended stripline design. Now, much of the field lines are in the air sections above and below the substrate, with much less field being within the dielectric and experiencing dielectric losses.

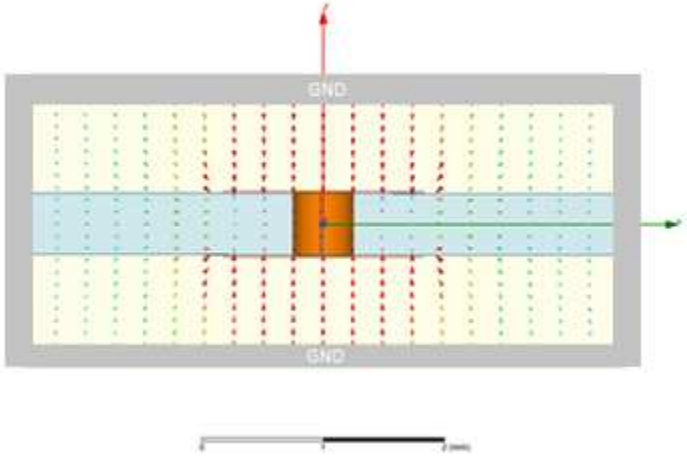

Figure 4 – Double Sided Suspended Stripline with Rogers RO 4003C Substrate

Figure 4 shows a cross-sectional view of the proposed Double Sided Suspended Stripline. We can see that the field lines are very strongly confined to the air regions within the design, more so than in a standard suspended stripline design.

To evaluate the different performance characteristics, ADS was used to simulate each transmission line geometry. Using ADS Momentum, a geometry was constructed for each design and a 2.5 dimension simulation was run to analyze the different performance metrics. The term"2.5 dimensional simulator" is a term of art and not a precise mathematical statement. In ADS the term 2.5D simply means that the software will simulate vertical vias as well as planar traces.

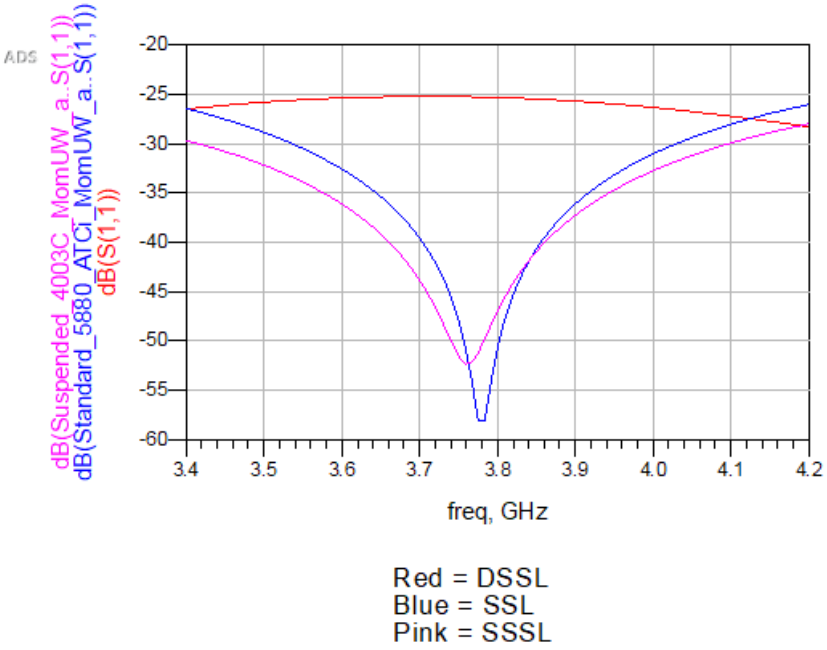

Figure 5 – Reflection Coefficients

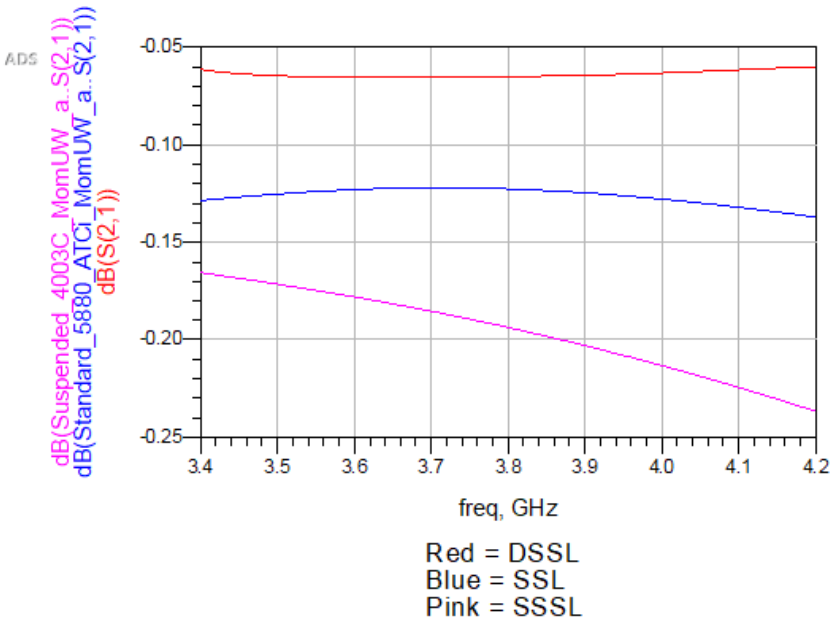

Figure 6 – Transmission Coefficients

From the above figures we can see that the DSSL design does in fact show a marginal improvement in transmission when compared to SSL and SSSL. Figure 5 shows the reflection coefficient Γ, or S(1,1), of each design. The reflection coefficients for each design are well below -20dB and for all practical purposes Γ is zero. Figure 6 provides the primary figure of merit used throughout this thesis which is the transmission coefficient T, or S(2,1). From the figure, there is an obvious improvement of about a tenth of a dB per wavelength in the DSSL design over the other two designs. The SSL simulated above utilizes a much higher performing, higher cost substrate (Rogers Duroid 5880), while the SSSL and DSSL simulations use a much cheaper substrate (Rogers RO 4003C).

Literature Review

Researchers at the University of Electronic Science and Technology of China introduce the use of DSSL, which they call Double Substrate Integrated Suspended Line (DSISL), for high Q spiral inductors. The paper addresses the same problems in microwave transmission media that have already been covered in this thesis; dielectric and resistive ohmic loss. The fabrication process outlined is the same as well; drilling a plated through-hole via through the center of the conductors. However, their primary goal was to reduce losses for the purpose of increasing quality factor. The paper drew the same conclusion that a double sided line outperforms suspended stripline and microstrip line in terms of loss and maintaining signal integrity. [10]

Other research utilizes DSSL for resonators to achieve high unloaded-Q in diplexers. Again, dielectric and conductor losses were cited as the limiting factor in diplexer design. The paper supports the evidence in this thesis that dielectric loss can be substantially reduced by utilizing a DSSL design and, in the application of diplexers, much better frequency selectivity could be obtained due to the improved Q-factor. [11]

Reference [12] provides a different approach to the use of double sided transmission designs. A double sided stripline with an inserted conductor plane was proposed for the purpose of reducing the size of the overall circuit. The conductor plane inserted between the traces serves as a virtual ground that isolates the two signal traces essentially allowing two separate microwave circuits to be made within the same physical

space. The paper successfully implemented this design to create a bandpass filter with two transmission zeros.

The references listed above provide niche design applications for DSSL but do not describe a design process for designing simple DSSL transmission lines. This thesis will develop design equations through empirical results on how to design a 50Ω line and how to apply it to different applications, with the specific application of this thesis being a planar orthomode transducer. This thesis will support the results of other published research and expand on the design potential of double-sided suspended stripline. The results provided in the following sections continue to demonstrate the merits of double sided stripline compared to other microwave transmission media.

2 BACKGROUND FOR THE RESEARCH

Antenna Technology Communications Incorporated (ATCi)

The goal of this research is to create an improved version of the existing planar orthomode transducer (OMT) utilized by Antenna Technology Communications Inc (ATCi) for some of their Simulsat products. A secondary goal is to make the design as cheap to build and implement as possible using available fabrication techniques. This new design has lower losses while maintaining polarization isolation between orthogonal wave components. The function of an orthomode transducer is to separate orthogonal wave components at the receiver, which allows us to take advantage of polarization diversity — transmitting two signals on the same frequency but orthogonally polarized, and then separating and down-converting them at the receiver. Figures 7 and 8 are a visual representation of polarization diversity. This effectively allows for twice as many channels to be transmitted. This design is operating at C-band and the bandwidth being used is from 3.4-4.2GHz.

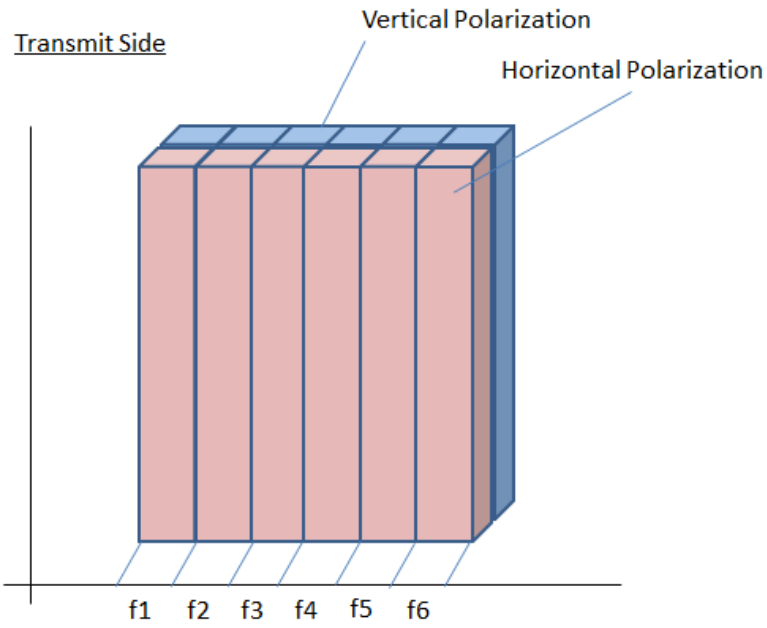

Figure 7 – Cross Polarized Channels Transmitted at the Same Frequency

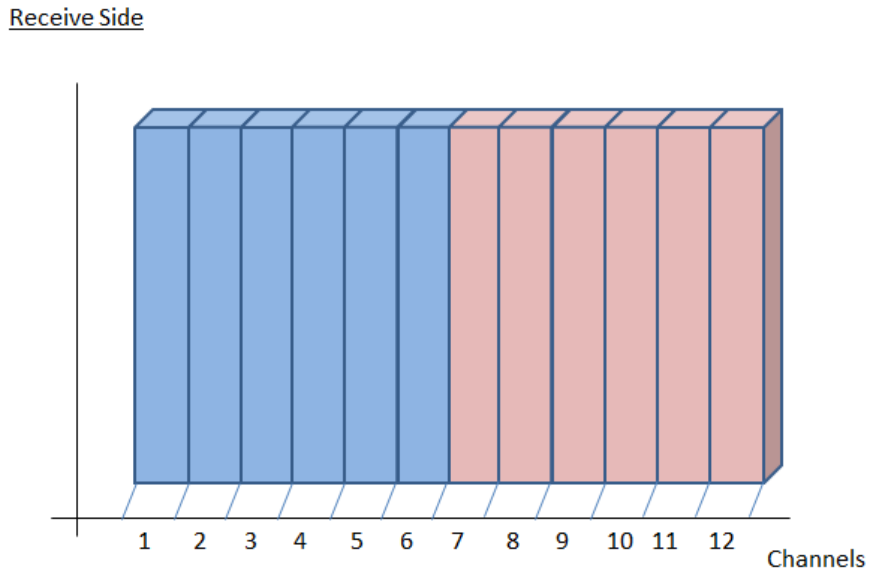

Figure 8 – Channels After Separation and Down-conversion

The Simulsat antenna is a parabolic torus reflector that is used to capture signals from multiple satellites and focus them into an array of as many as 34 horn feeds. The 34 horn feed arrangement offers a more efficient use of space over a multiplicity of conventional parabolic reflectors that each utilize only one horn feed. In essence, a single Simulsat has the capacity of 34 individual parabolic reflectors in a significantly smaller footprint. Figures 9 and 10 show the Simulsat Antenna and the feed network associated with each individual horn.

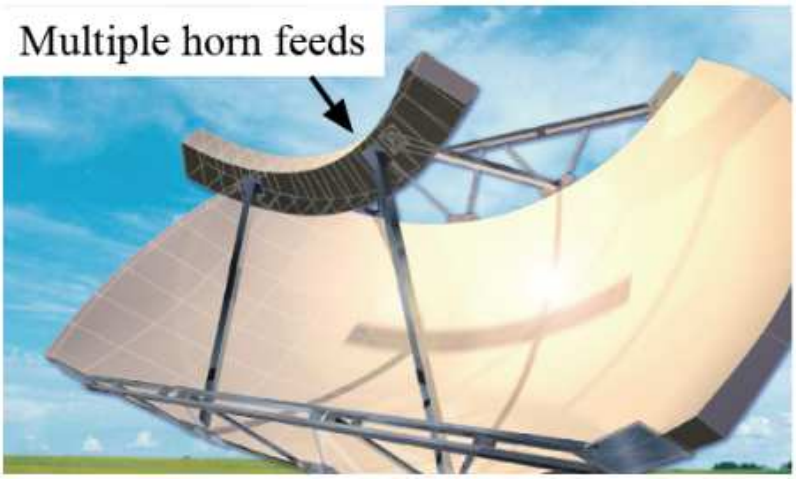

Figure 9 – Simulsat

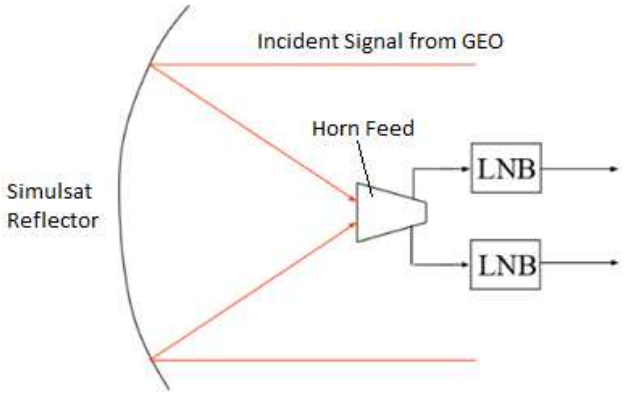

Figure 10 – Receiving Network

The orthogonally-polarized signals are separated by the OMT and routed to a Low Noise Block, which amplifies the signal and down converts the channels which are sent via coaxial cable to the receiver equipment. It is crucial that as high of a signal-to-noise ratio as possible is maintained during the wave component separation prior to the first low noise amplifier stage. Lower losses means higher signal integrity, higher picture resolution, faster streaming capabilities, and also provides a more reliable communications link. Figure 11 shows the block diagram of the LNB which includes a low noise amplifier, local oscillator, mixer, and band pass filter.

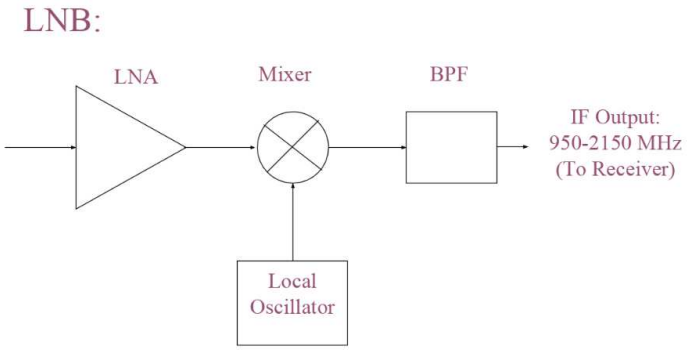

Figure 11 - Block Diagram of the Low Noise Block

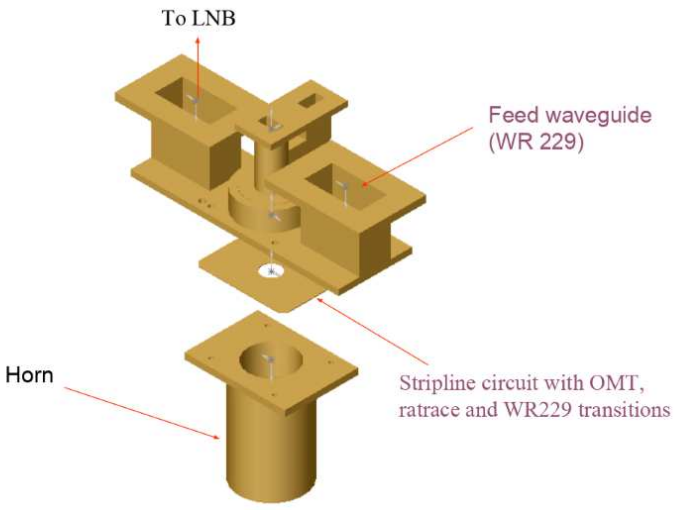

Figure 12 – Mechanical Structure of the Feed Network

From Figure 10 we can see that the planar orthomode transducer is sandwiched between the feed horn and the LNB's.

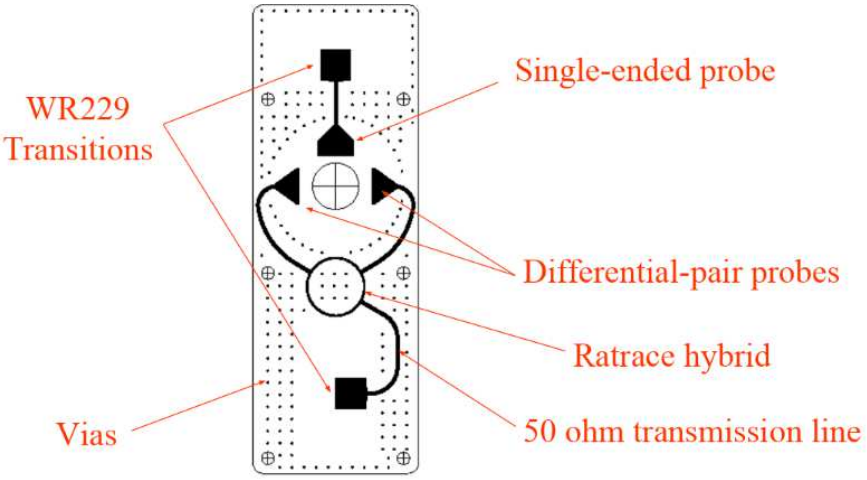

Figure 13 – Top View of the Planar OMT

The planar OMT shown in figure 13 consists of a single-ended probe, a differential pair probe, and two WR229 waveguide transitions (one for each polarization). The single-ended probe picks up one polarization while the differential probes pick up

the orthogonal polarization. The combination of a differential pair for one polarization and a single-ended probe for the other polarization allows for greater isolation between the polarizations than is possible using single-ended probes for both. Additionally, compared to using two differential pairs, the combination results in a much simpler feed network that can be realized on a single layer. Because the circular C-Band horn itself supports multiple TE11 waveguide modes, as shown in figure 14, it is crucial to maintain signal isolation between the polarizations.

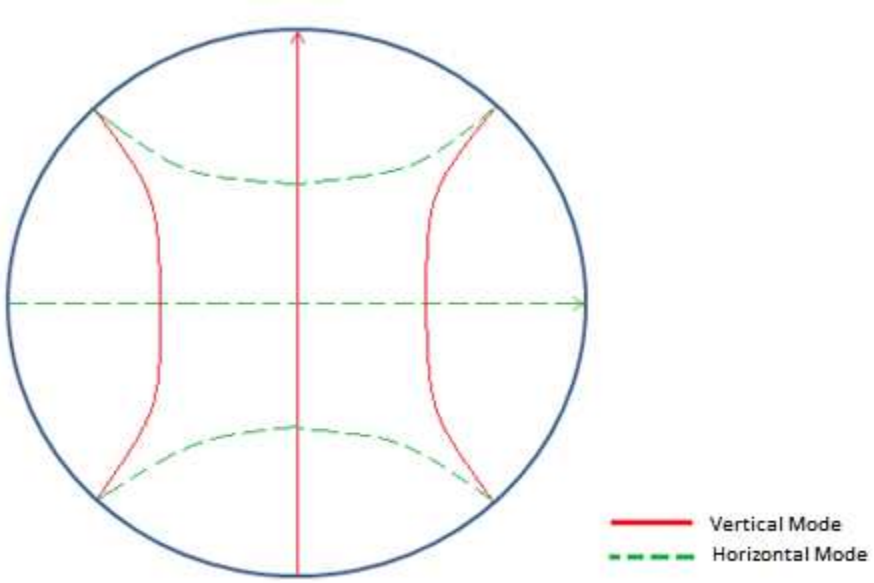

Figure 14 – Circular Waveguide Vertical and Horizontal Modes

To convert the differential signal to a single ended signal, a balun must be implemented. A Ratrace Hybrid is used as a balun in this design and will continue to be used in the new and improved design. The two signals received on the orthogonal polarizations are then routed to probes that transition the signals into the WR229 waveguides, each of which fees into an LNB.

3 STRUCTURE MODELING AND SIMULATION

Materials

One of the goals of this design is to reduce cost compared to ATCi's current design. The current design uses Rogers Duroid 5880 as its primary dielectric, which is a very high quality and high performing material, but is orders of magnitude more expensive than common dielectrics like FR4.

The double-sided stripline design will use Rogers 4003C, which is on the order of 5 times cheaper* than Duroid 5880 and also has fairly high quality performance. This material offers a good trade-off between cost and performance and, when used in suspended stripline transmission medium, outperforms higher quality materials utilized in standard stripline design.

Material	ε_r	tanδ
FR4	4.5	0.008
Rogers RO4003C	3.55	0.0027
Rogers RT Duroid 5880	2.2	0.0009

Table 1 – Values of Relative Permittivity and Loss Tangent for Different Materials [13-14]

*For 0.020" thickness, half-ounce copper cladding on both sides, 18" x 24" size, for quantities between 14-49
RO4003C = $67.84/panel
Duroid 5880 = $348.69/panel
Quoted by Dale Doyle, Applications Development Manager, Rogers Corporation, 02/11/2019

Geometry

The geometry of DSSL is what makes it a viable alternative to standard stripline or microstrip for low loss applications. In the DSSL geometry shown in figure 15, most of the electric fields lines propagate through lossless air medium instead of lossy dielectric medium. The geometry of DSSL is very similar to that of standard suspended stripline—the major difference being that DSSL utilizes two traces on eithr side of the supporting substrate connected with vias. Essentially, this design is an upgraded form of standard SSL.

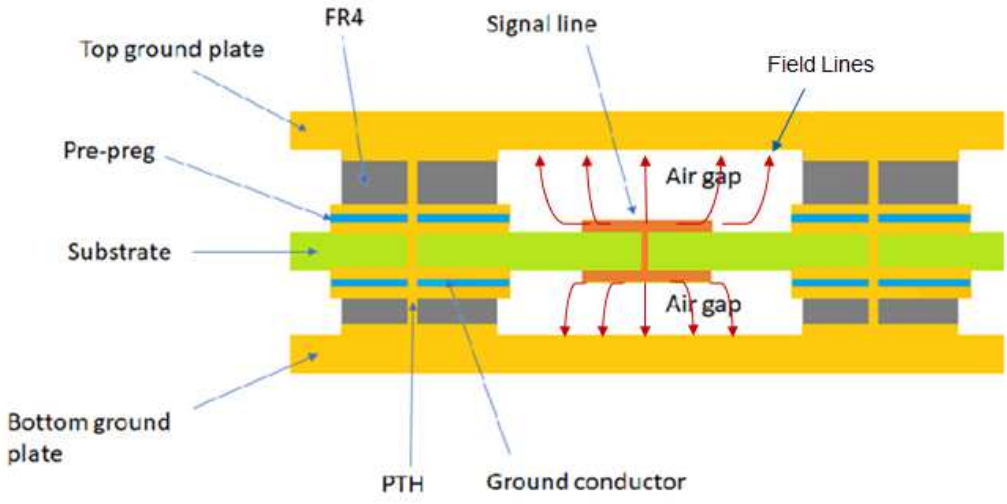

Figure 15 – Representative Cross-sectional View of the DSSL Design

The supporting substrate should be realized using the smallest dielectric thickness practical in order to reduce the dielectric loss as much as possible. Rogers Corporation offers boards as thin as 5mil (0.005”) but these boards can warp, bend, and tear easily. Since this design will be used outdoors the board itself should be reasonably sturdy. For

that reason it was decided that a 20mil board would result in the significant dielectric loss while still maintaining mechanical integrity.

Plated vias with 20 mil diameter are used to ensure that the top and bottom signal conductors are electrically connected. Additional plated vias are used to connect the top and bottom ground planes. In both cases, at least 10 vias per wavelength are required so parasitic parallel plate modes are not excited between the top and bottom conductor.

The substrate itself will be supported by FR4 boards as pictured in Figure 15.

Transmission Line Simulation

The design process was started in ADS Momentum by defining the structure dimensions as shown in figure 16. These dimensions were chosen to emulate the current OMT dimensions as best as possible. However, in order for the structure to achieve best performance two main parameters need to be optimized: the width of the trace and the air-gap spacing above and below the substrate. Figure 17 shows the view of DSSL in ADS Momentum with top and bottom conducting layers, as well as vias.

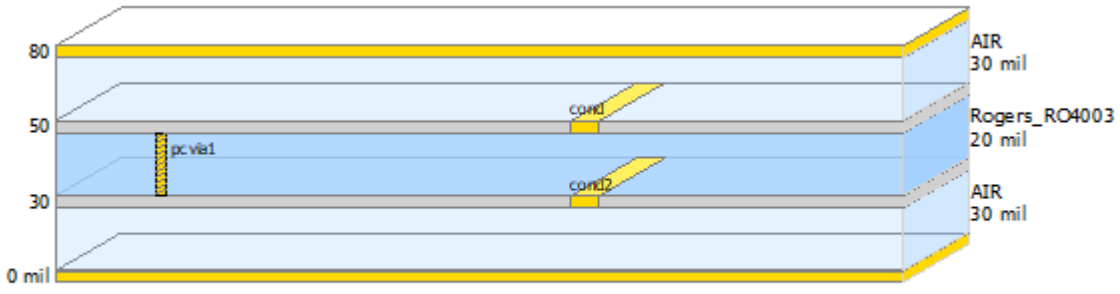

Figure 16 – ADS Stack-up with Conductor and Via Layers

Figure 17 – Top View of the Transmission Line in ADS Momentum with Conductor and Via Layers

From figure 15, we can see that the spacing above and below the board is determined by the thickness of the FR4 boards used to support it. These boards come in predetermined thicknesses so the air-gap spacing must conform to what is available. Spacing of 20mils, 30mils, and 40 mils were used to derive the optimal air-gap spacing.

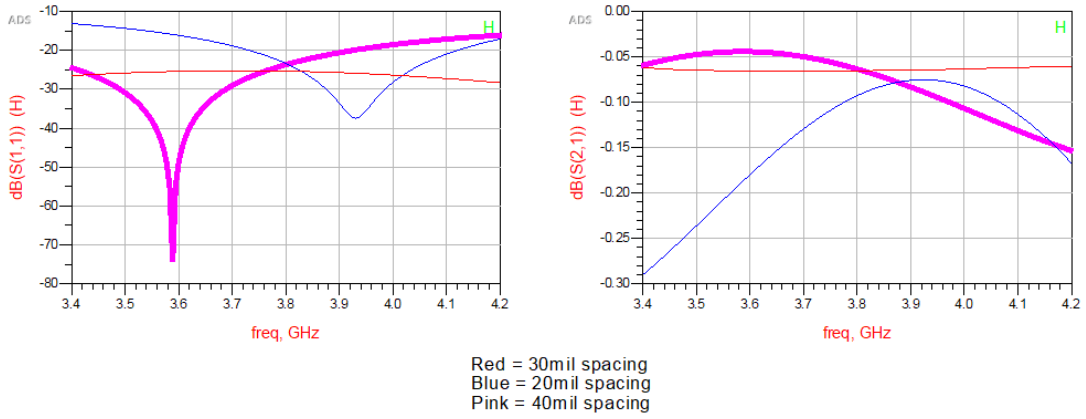

Figure 18 – Simulation with Different Air-gap Spacing

From figure 18, the optimal air-gap spacing that can be realized with readily available board thicknesses is 30 mils. The optimal width of the 50Ω DSSL trace was found through rigorous and iterative simulation and is 65mils at this frequency. The reflection and transmission characteristics of the optimal width are shown in figure 20. . Six different simulation examples were analyzed utilizing the same substrate thickness and air gap spacing but with different substrate materials. The optimal DSSL width was

found for each example and an empirical equation was created to try to reproduce the optimal width as best as possible.

Design Number	Substrate Material	effective_e	Optimal SSL Width(mil)	Optimal DSSL Width (mil)	From Equation (mil)
1	Rogers RO 4003C	1.318	102	65	63
2	Rogers RT/Duroid 5880	1.203	100	63	63
3	Rogers RO 4350B	1.325	101	65	65
4	Rogers 3010	1.991	67	45	58
5	Rogers RT/Duroid 6006	1.455	93	61	62
6	Rogers RT/Duroid 6010	1.992	67	45	58

Table 2 – Design Examples Used to Derive Optimal Width Equation

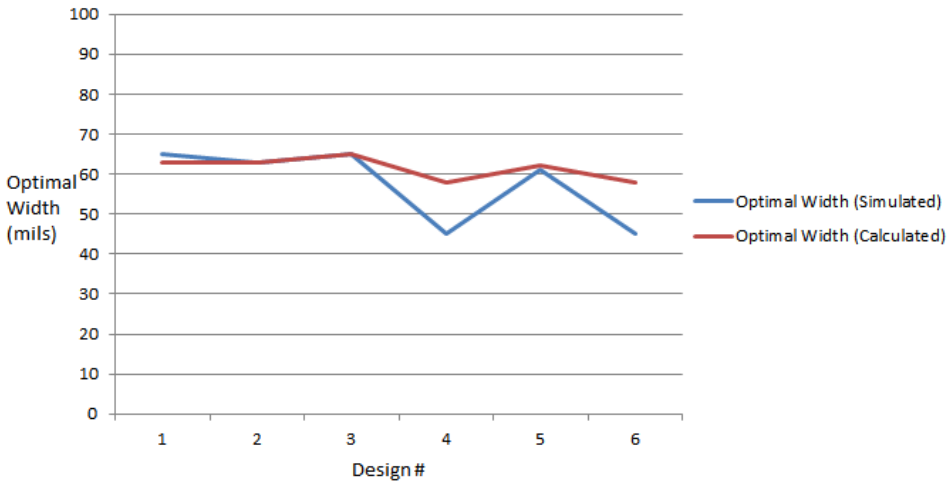

Figure 19 – Optimal Widths for Design Examples (Simulated vs Calculated)

Figure 19 shows the calculated optimal width using the empirically derived equation and the optimal width found through simulation. The equation is quite accurate except for a few cases where the calculated width and simulated width vary by a

relatively small amount (about 10 mils). For the most part the equation gives a very good starting point for optimization. Equation 1 shown below can be used to determine a close aprozimation for the optimal width of a DSSL. The equation uses parameters that can be evaluated easily in LineCalc in Keysight ADS or any other analytic tool.

$$\left(\sqrt{\frac{\varepsilon_{e_{SSL}}-1}{\varepsilon_{r_{SSL}}+1}}\right) * \left(W_{SSL}(mm)\right) + 0.968 = W_{double}(mm)$$

Equation 1 – Optimal Width for 50Ω DSSL Transmission Lines

The SSL subscript denotes values from standard suspended stripline as found in LineCalc (effective permittivity, relative permittivity, and optimal width in millimeters). The standard suspended stripline design should have the same material definitions and the same dimensions as the desired DSSL. These known values can then be used to derive a close approximation for the optimal width of DSSL.

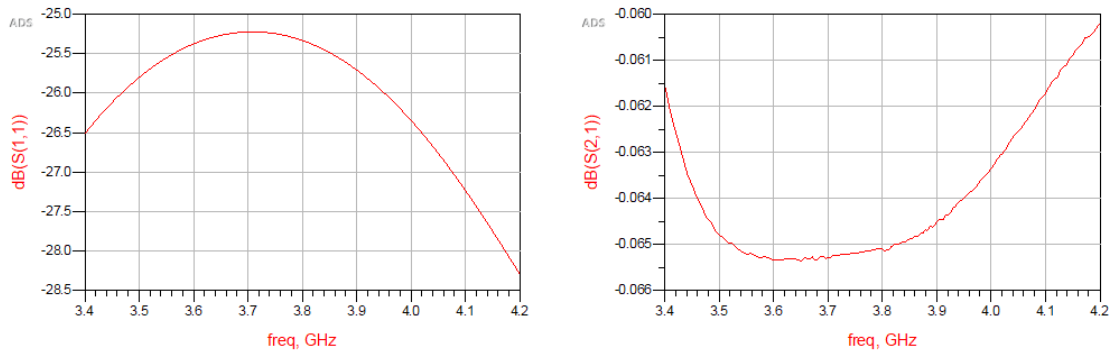

Figure 20 – Reflection and Transmission Responses of DSSL with Optimal Width

In order to demonstrate that the optimal trace width and air-gap spacing found in ADS Momentum are true and accurate, the design was recreated and simulated in Ansys HFSS. Figure 21 shows the 3D model of DSSL in HFSS.

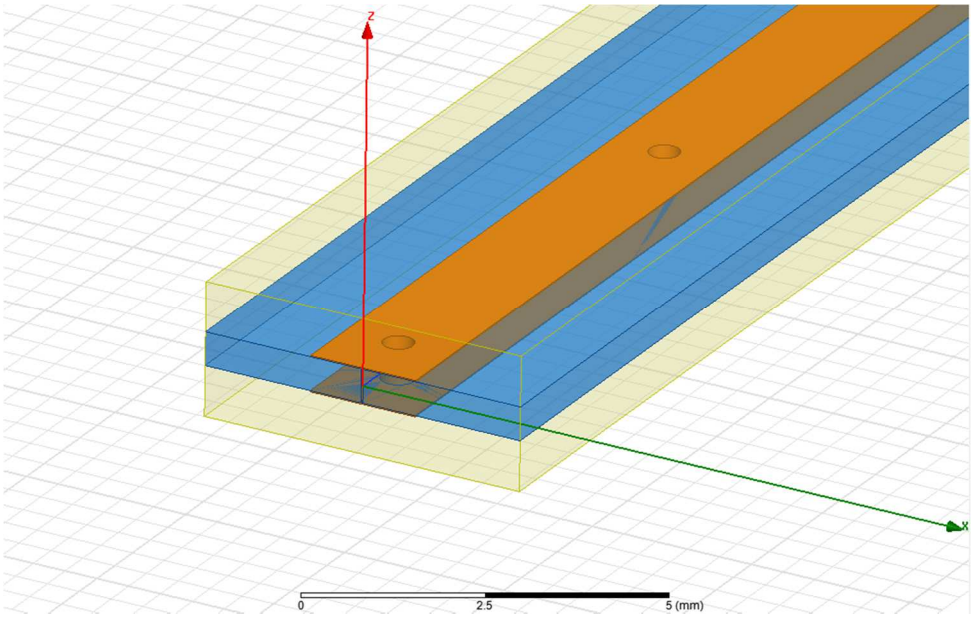

Figure 21 - DSSL Model in Ansys HFSS

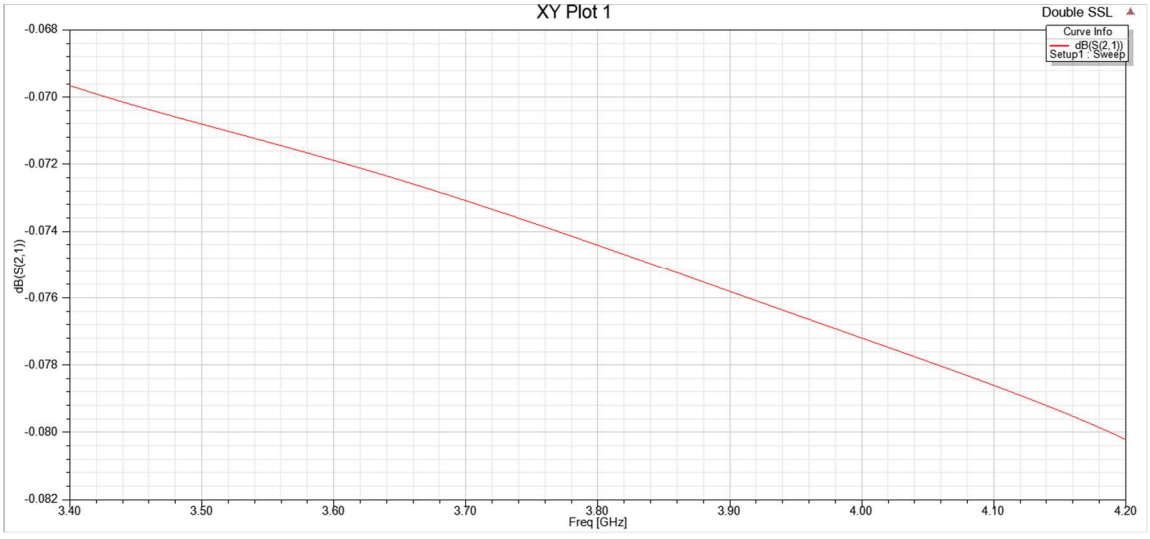

Figure 22 – Transmission Response of DSSL Model Obtained from HFSS

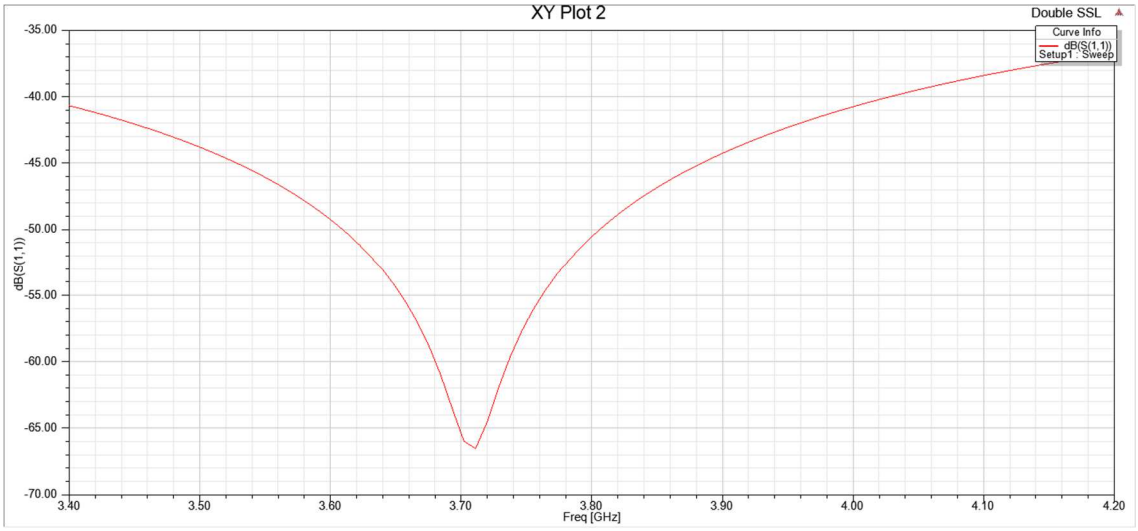

Figure 23 – Reflection Response of DSSL Model Obtained from HFSS

Figures 22 and 23 show the transmission response and the reflection response of the DSSL line simulated in HFSS, respectively. The transmission response from HFSS is about 0.01dB lower than the corresponding ADS results. The reflection response from HFSS is below -40dB (essentially Γ=0). Figures 20, 22, and 23 are all in reasonable agreement and prove the width and spacing of the design to be optimal and accurate.

Rat-Race Hybrid Simulation

Now that a standard transmission line has been optimized, the balun must also be optimized. For this design a directional coupler called a rat-race hybrid is used as a balun to convert the differential signal into a single ended signal. The S-parameter matrix for an ideal rat-race hybrid is shown below [15].

$$[S] = \frac{-j}{\sqrt{2}} \begin{bmatrix} 0 & 1 & 1 & 0 \\ 1 & 0 & 0 & -1 \\ 1 & 0 & 0 & 1 \\ 0 & -1 & 1 & 0 \end{bmatrix}$$

Figure 24 – Ideal Rat-race S-matrix

From the ideal S-matrix, the rat-race should provide perfect isolation between ports 1 and 4, a half-power split and 90 degree insertion phase change from port 2 to port 4, and a half-power split and -90 degree insertion phase change from port 2 to port 1. This will create an equal power split and 180 degree phase difference between the signals at ports 4 and 2. However, in this application the signals will be incident at ports 4 and 1, and will be combining in phase at port 2.

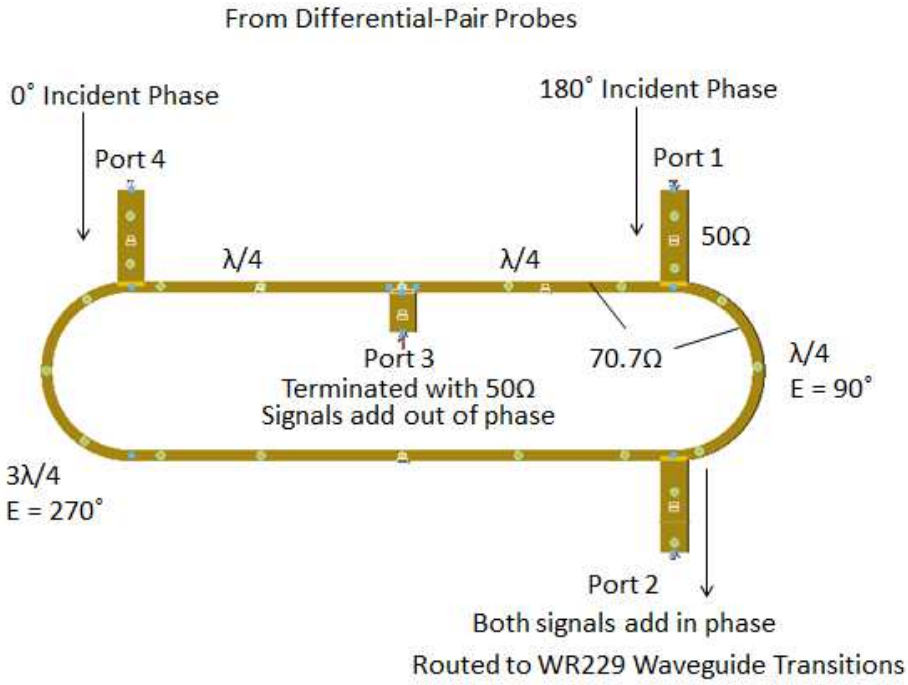

Figure 25 – Rat-race Hybrid in ADS Momentum

Figure 25 shows the rat-race layout in ADS Momentum with respective impedances and line lengths. The shape of this rat-race is not circular like most conventional rat-race hybrids. The "elliptical" shape was used for this design with the intention of minimizing the amount of vertical space that the rat-race took up, with the overall goal being to make the length of the planar OMT shorter. The characteristic impedance of the rat-race is $Z_0\sqrt{2}$, or 70.7Ω in a 50Ω system. The width of the DSSL trace must be re-optimized for this new impedance using the same iterative process as before for the 50Ω line. Furthermore, the trace lengths shall be either 90 or 270 electrical degrees. This will ensure that the signals add up in phase at port 2. From ADS Momentum, the optimal width of a 70.7Ω line is 28mils, with a 90˚ electrical length of 640mils as shown in figure 26.

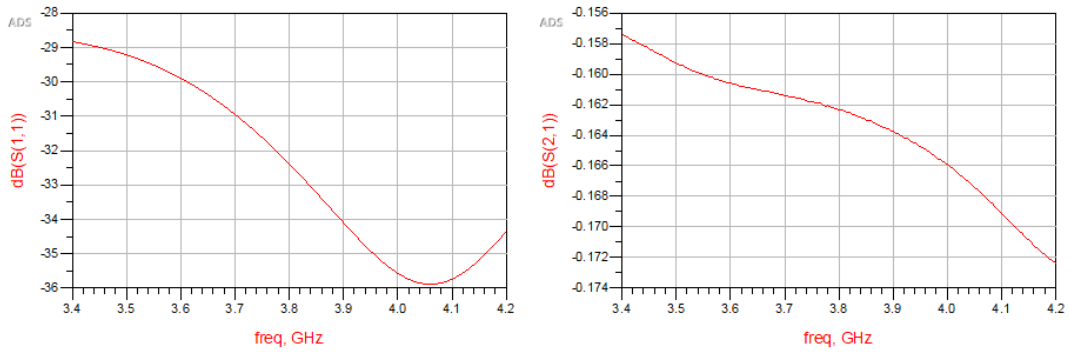

Figure 26 – Reflection and Transmission Responses for Optimal Width of a 70.7Ω line

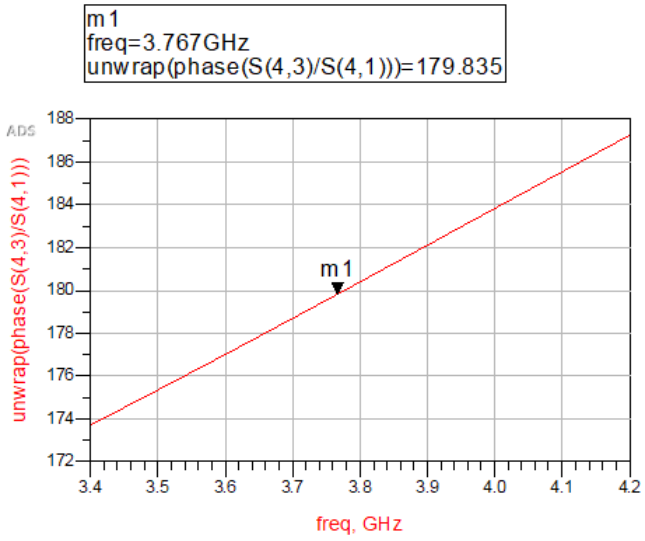

Figure 27 – Phase Difference Between Ports 1 and 4 of a Rat-race Hybrid

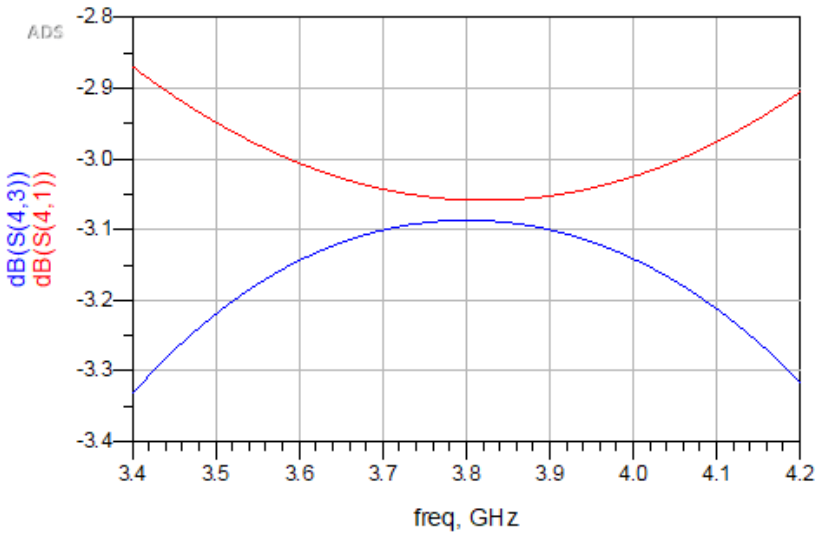

Figure 28 – Equal Power Split Between Ports 1 and 4

Figure 26 shows magnitudes of the reflection and transmission responses of the 70.7Ω line in ADS. The magnitude of S(1,1) is below -30dB (essentially Γ=0) and the magnitude of S(2,1) is about -0.165dB. The losses in the 70.7Ω are higher than the losses in the 50Ω. This can be attributed to the additional ohmic losses present in a higher

impedance system. Figures 27 and 28 show almost exact 180˚ phase difference and an almost perfectly equal 3dB power split at the center frequency for the Ratrace hybrid. The equal power split is slightly less than 3dB at the center frequency due to losses in the system. There is also the typical variation of the power split versus frequency seen in Ratrace hybrids.

In ADS Momentum the ports are assumed to be at a zero-phase offset relative to each other, so the end result is that a 180˚ phase difference will be observed at port 2. In the planar OMT, however, ports 1 and 4 are initially 180˚ out of phase relative to each other and the end result should be an observation of 0˚ phase difference at port 2. The ability to define ports with an initial phase offset is not possible in ADS Momentum so to observe the 0˚ phase at port 2, Ansys HFSS will be used. This simulation will also help validate the optimal trace width and electrical lengths found in ADS. Figure 28 shows the 3D model of the rat-race hybrid in HFSS.

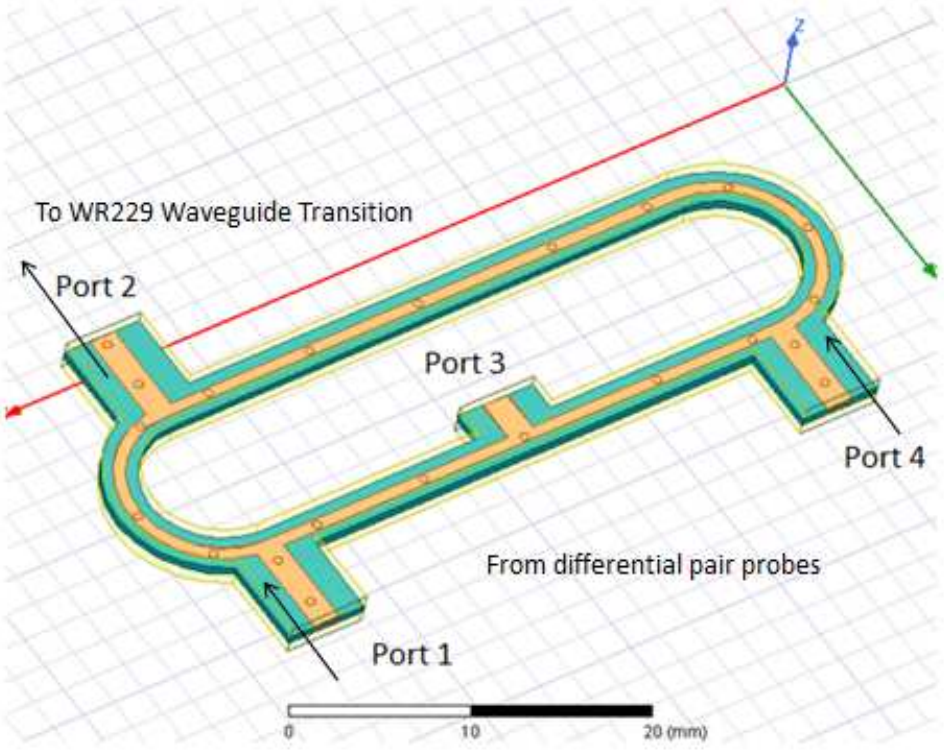

Figure 29 – Rat-race Model in HFSS

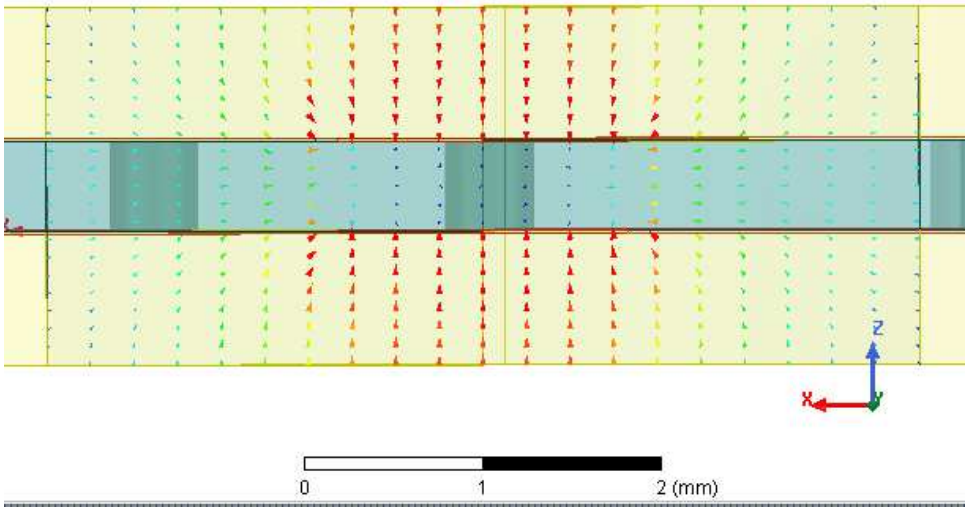

Figure 30 - Port 4 (0 Degree Incident Phase)

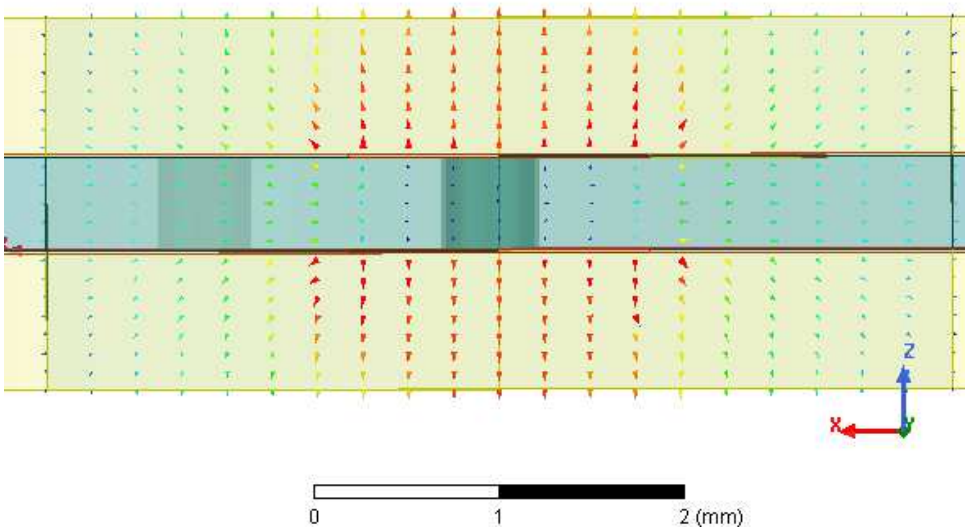

Figure 31 - Port 1 (180 Degree Incident Phase)

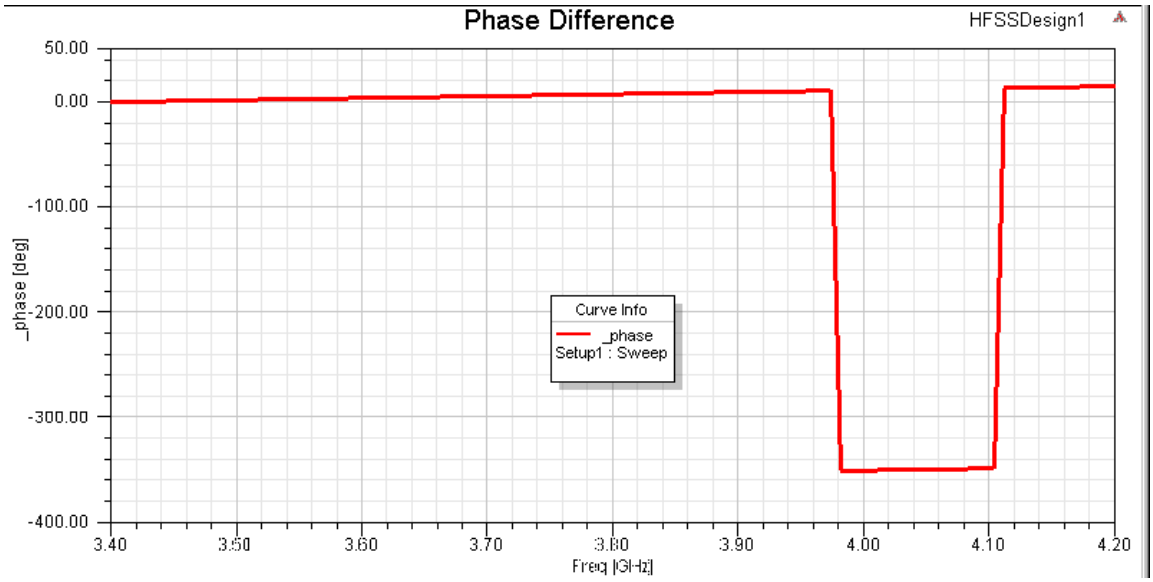

Figure 32 – Phase Difference at Port 2

Notice in figures 30 and 31 that the electric field lines are pointing in opposite directions. This was done by defining the integration lines at the ports in

opposite directions to produce the initial 180˚ phase offset. From figure 32, the signals do in fact add up at 0˚ phase at port 2 with about 10˚ of error across the bandwidth.

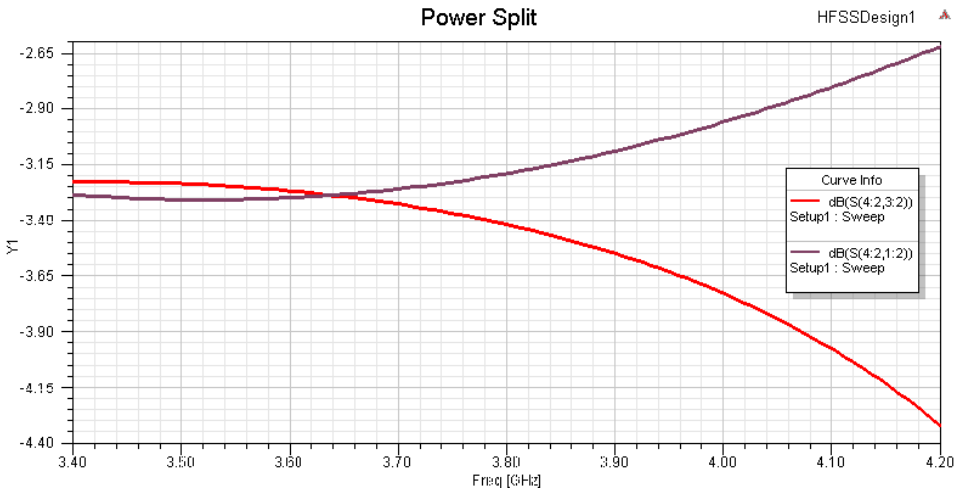

Figure 33 – Power Split

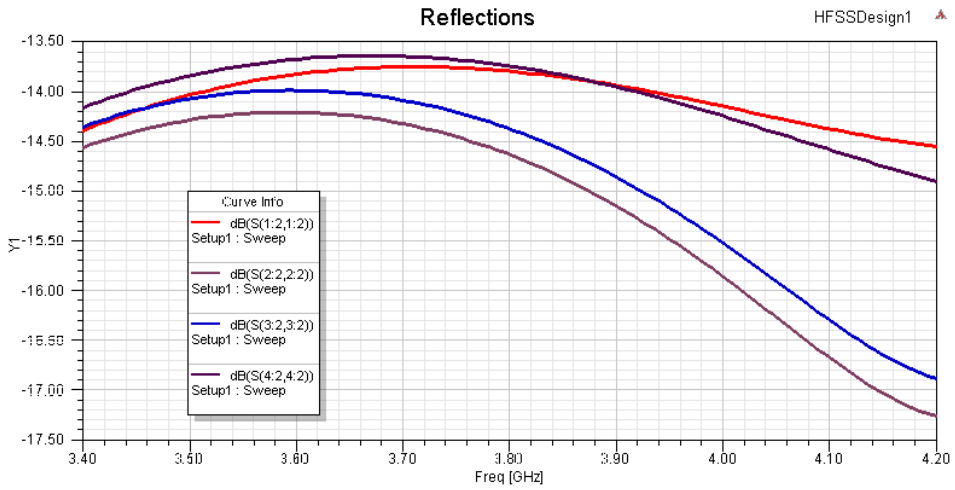

Figure 34 – Reflections at Each Port

Figure 33 shows the power split. Figure 34 shows the reflections at each port. The reflections for each of these ports are somewhat worse than a transmission line by itself. Figures 27, 28, 32, and 33 are all in reasonable agreement and demonstrate that the line lengths and widths for the Ratrace hybrid are more or less optimized.

Probe Optimization

From figure 13, there are 3 different stripline-to-waveguide probes that need to be optimized for maximum signal transfer: the WR229 transitions, the differential-probe pair, and the single-ended probe. These optimizations can be done using the optimization tool in Ansys HFSS, as shown in figure 34. The goal is to optimize the probe dimensions to produce a reflection coefficient of less than -10 dB ($\Gamma < -10dB$) over the desired frequency range. In the following sections, the DSSL probe responses will be compared to the probe responses of the standard stripline design currently used by ATCi in their planar OMT design.

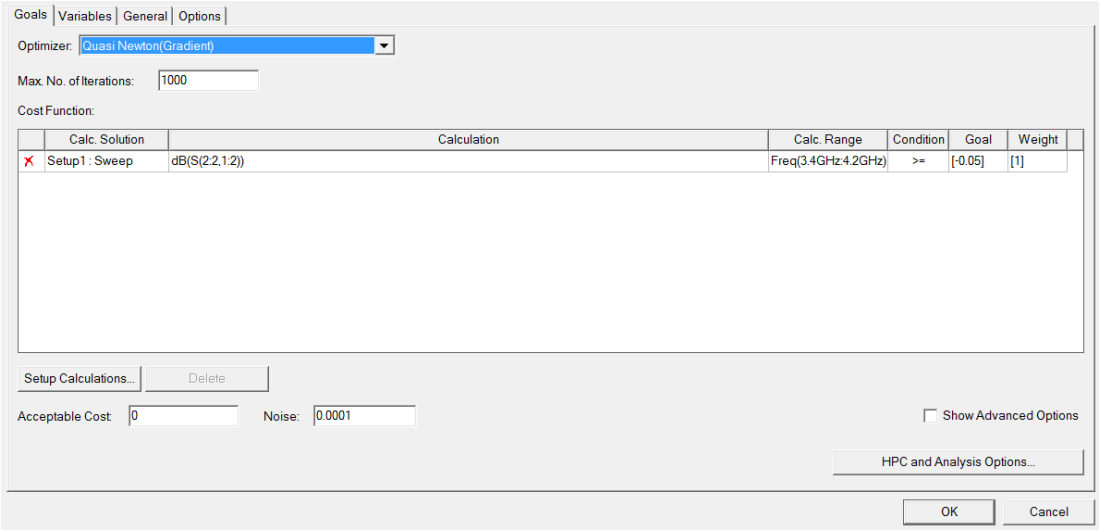

Figure 35 – Optimization Set-up in HFSS

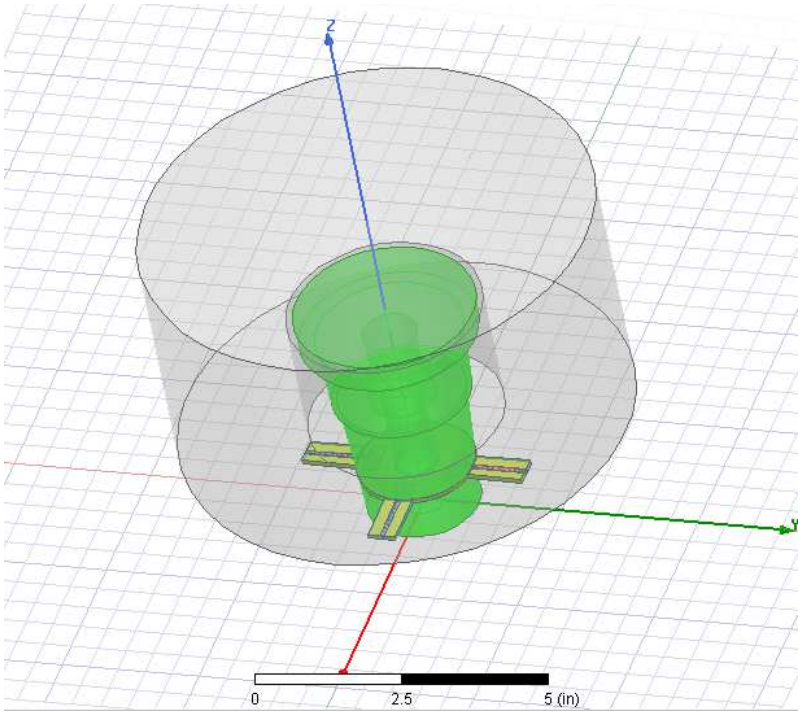

Figure 36 - HFSS Model of the C-band Horn Feed with Single and Differential Probes

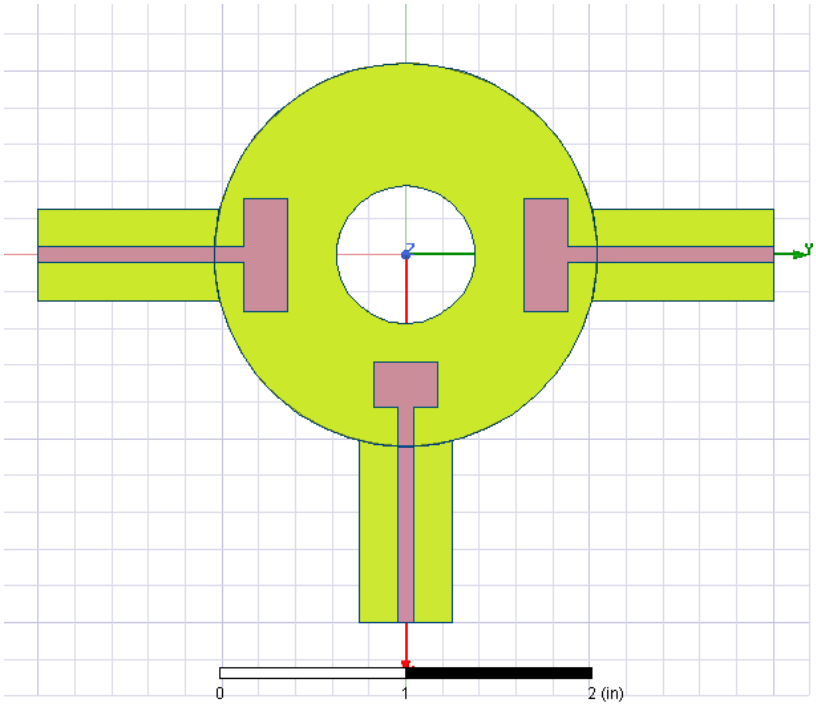

Figure 37 – Top View of the Single and Differential Probes

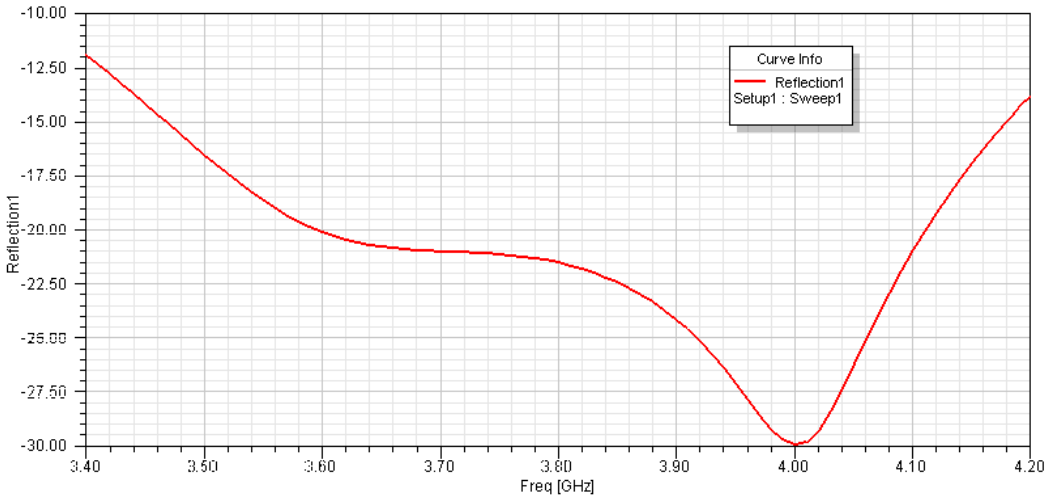

Figure 38 –DSSL S(1,1) for Differential Probes

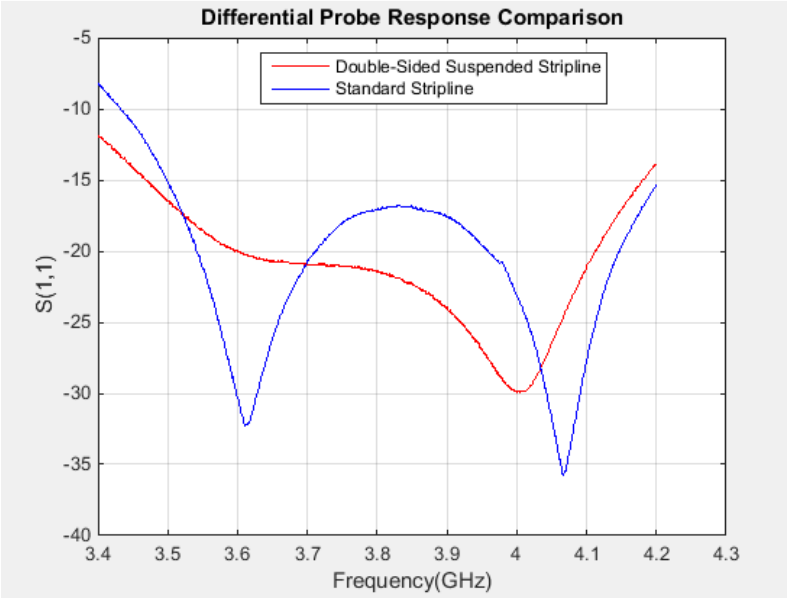

Figure 39 – Comparison of the Differential Probe Response Between SSL and DSSL

Figures 36 and 37 show the 3D model of the C-band horn in HFSS. Figure 39 shows a comparison of the magnitudes of the input reflection responses of the DSSL and SSL designs for the differential probe pair. The DSSL probes are below -15dB for most

of the bandwidth but do not exhibit the sharp resonances seen in the SSL response. Both designs are still comparable in terms of performance.

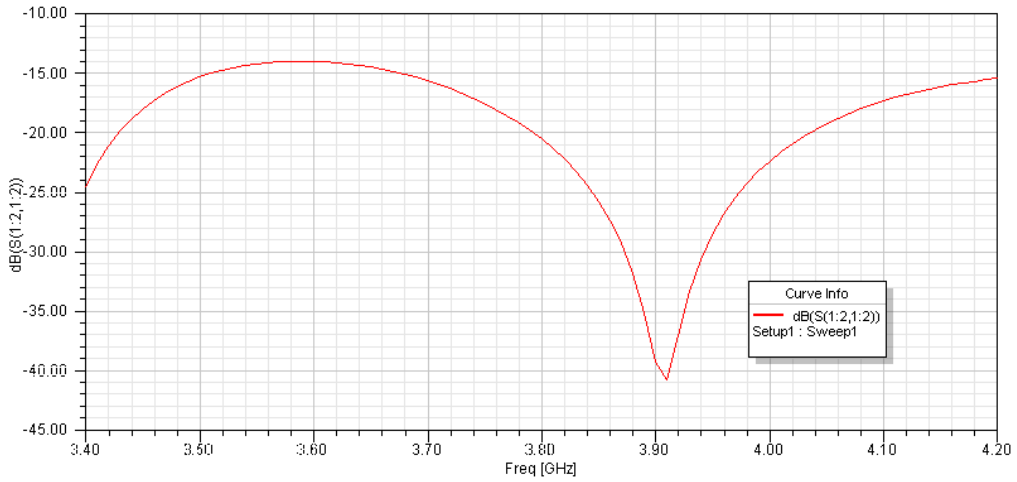

Figure 40 – Reflection Response for Single-Ended Probe Realized in DSSL

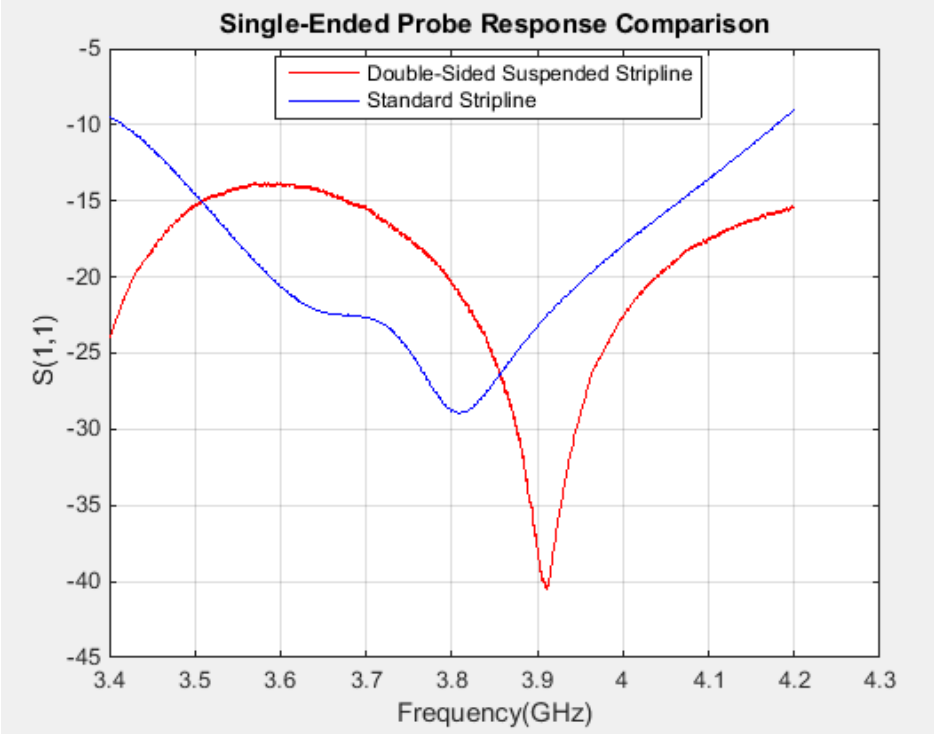

Figure 41 - Comparison of the Single-Ended Probe Response Between SSL and DSSL

Figure 41 shows a comparison of the magnitudes of the reflection response for each design for the single-ended probe. The DSSL probe is well below -15dB for most of the bandwidth and exhibits a sharp resonance close to the center frequency. The DSSL probe outperforms the SSL probe over about half of the bandwidth.

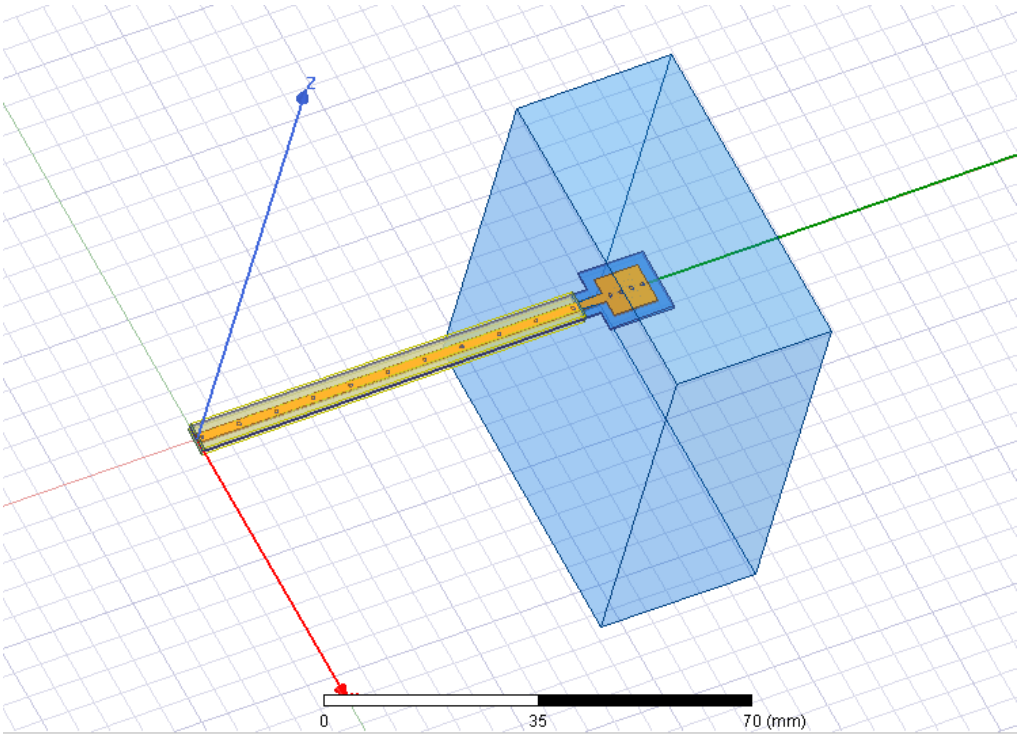

Figure 42 – HFSS Model for WR229 Waveguide Transitions

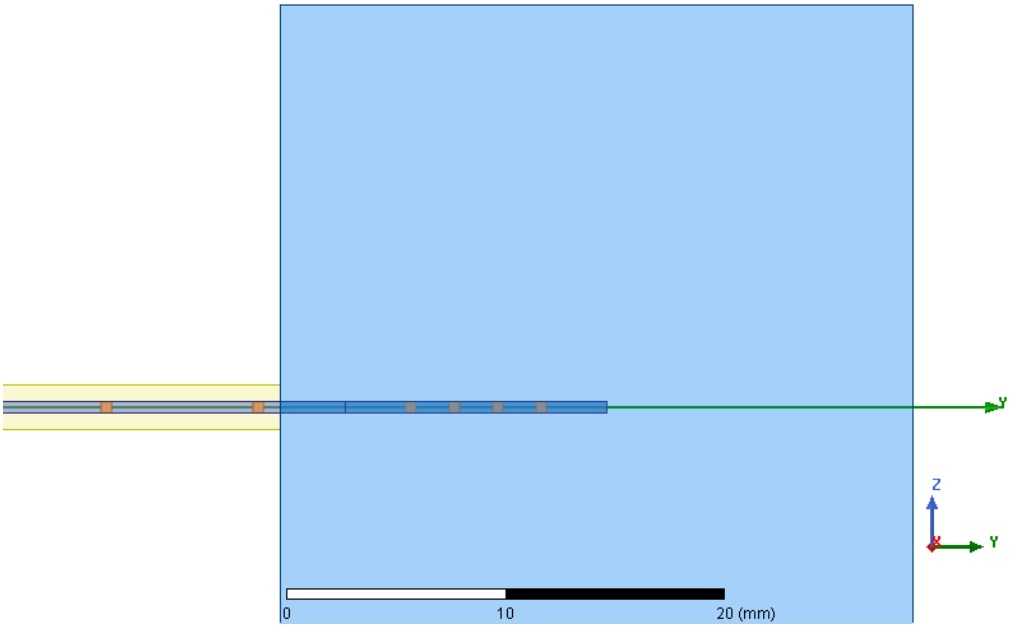

Figure 43 – Side View of WR229 Waveguide HFSS Model

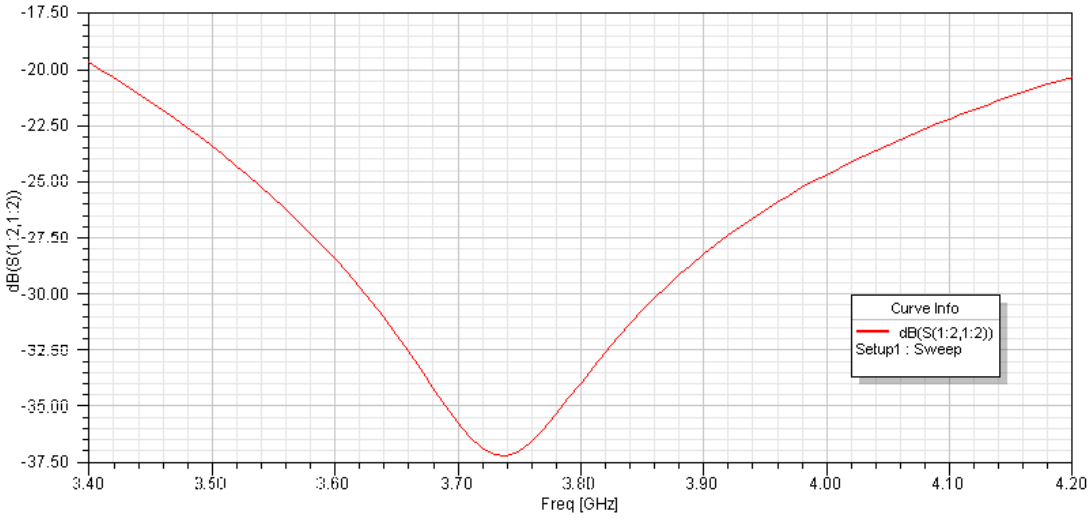

Figure 44 – Reflection Response for Waveguide Probe Transition in DSSL

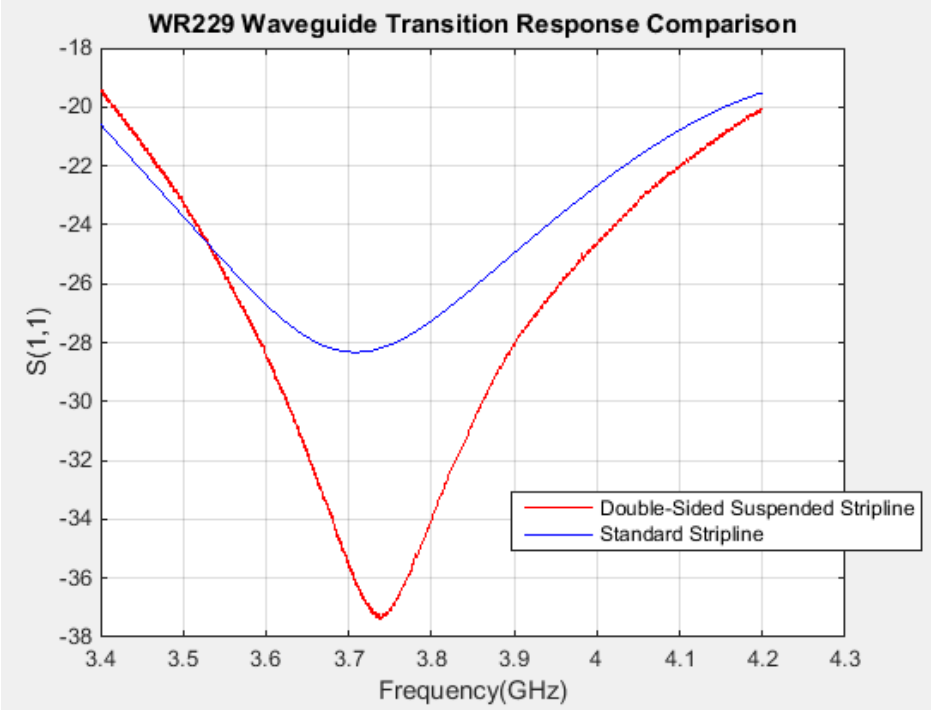

Figure 45 - Comparison of the WR229 Waveguide Probe Response Between SSL and DSSL

Figures 42 and 43 show the 3D HFSS model for the WR229 waveguide probe transitions. Figure 45 shows a comparison of the magnitudes of the reflection response for each design for the WR229 waveguide transition probes. The DSSL probe outperforms the SSL probe dramatically over the majority of the bandwidth. This behavior can be attributed to the fact that the DSSL probe is on a peninsula and there is less dielectric material in the waveguide transition. This same approach was not used for the single and differential probes because there is less structural support around them and the risk of the peninsula's bending or warping is much higher.

Figures 39, 41, and 45 show a comparison for each probe between the magnitudes of reflection response for the optimized probe dimensions for the DSSL versus the

optimized probe dimensions for the standard stripline design currently used by ATCi. In each case, a reflection coefficient below -10dB is achieved across the frequency band. In each case the performance of the DSSL design is comparable to, or better than, the performance of the standard stripline design.

High Frequency Performance

The high frequency performances of both SSL and DSSL were simulated in the frequency range of 1GHz – 40 GHz in HFSS. A fine mesh as shown in figure 46 was defined in HFSS in order to more accurately simulate the high frequency response of these geometries.

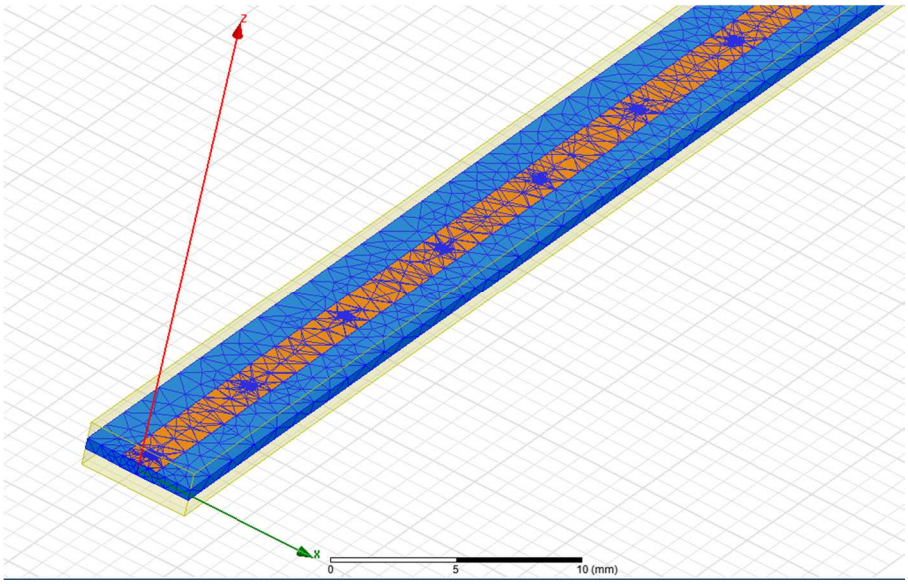

Figure 46 – HFSS Mesh for DSSL

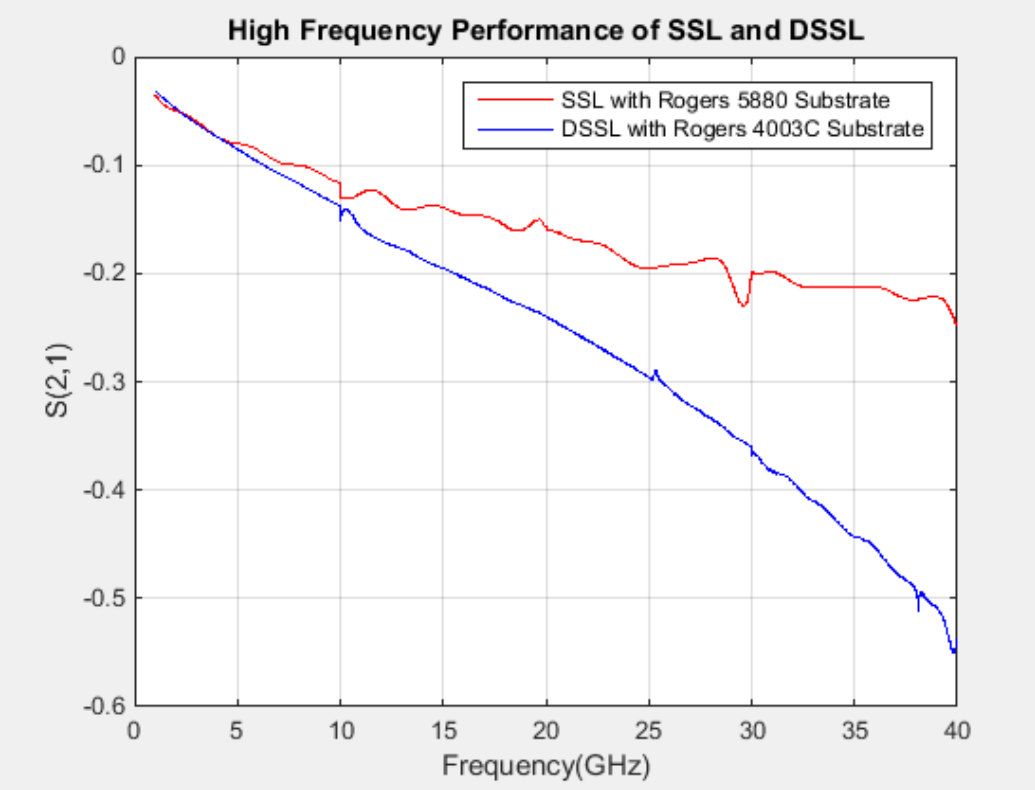

Figure 47 – Transmission Response for DSSL and SSL from 1GHz - 40GHz

Figure 47 shows the transmission responses of DSSL and SSL. The SSL utilizes the Rogers Duroid 5880 substrate and the DSSL utilizes a much less expensive Rogers 4003C substrate. Below 5GHz, the DSSL has about the same performance as the SSL. However, above 5GHz the performances of the designs begin to diverge from each other. The losses for the DSSL design increase quite rapidly above 10GHz while the SSL losses are less profound.

These results suggest that after about 10GHz, the geometry of the transmission medium itself is not sufficient enough to overcome dielectric loss. The substrate material will have the most effect on the losses through the line. The DSSL line could still

reasonably be used up to about 25GHz, but this depends on how much loss is acceptable in a system.

In the example of the planar OMT the maximum acceptable loss is -0.2dB (as defined by ATCi), so theoretically a planar OMT could be designed for X-band receivers (up to 12GHz). While the DSSL planar OMT cannot outperform an X-band waveguide OMT in terms of loss, the fabrication techniques involved are much simpler and cheaper than existing waveguide fabrication techniques [16-17]. If a few tenths of a dB of loss are acceptable in the receiving system, then a DSSL Planar OMT designed for X-band frequencies is a cheaper and simpler alternative to standard waveguide X-band OMT's. To put things in perspective using numbers, a quantity of 12 planar OMTs would cost about $1,950.00 *. For a quantity of 12 waveguide OMTs, the price would be about $17,010.00 [18]. If a company fabricates thousands, perhaps hundreds of thousands, of designs utilizing OMTs it is easy to see that a large amount of money could be saved by implementing planar OMTs over waveguide OMTs.

SMA - Microstrip - DSSL Transition

The dielectric and metal support structure around the DSSL makes it difficult to solder on SMA's directly for testing purposes. As a result, a microstrip line transition to DSSL is needed. The SMA can be easily soldered to a microstrip line which can easily be transitioned to DSSL. This will allow the DSSL circuit to be tested by a Vector Network Analyzer (VNA). It is also important to know what losses the microstrip transition and SMA contribute to the system. These losses, once simulated, can be de-embedded from

*Quoted by Bob Modica, Micro Circuits Inc. on 3/27/2019

the measurements obtained from a physical test board. This process will yield the actual thru losses of a DSSL transmission line.

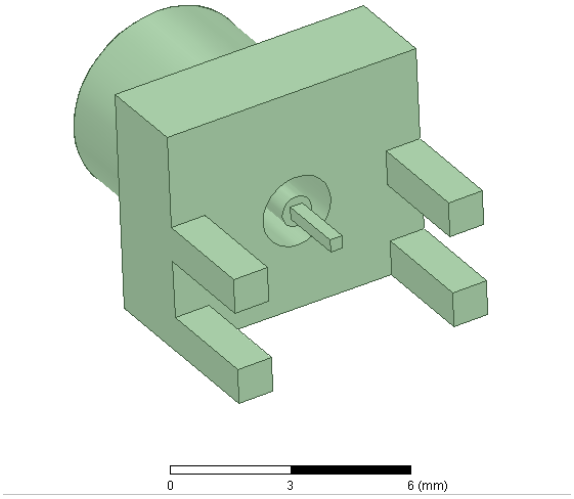

Figure 48 – SMA Model in HFSS

Figure 48 shows a surface mount SMA model that was created in HFSS using datasheets from Amphenol RF Division[19].

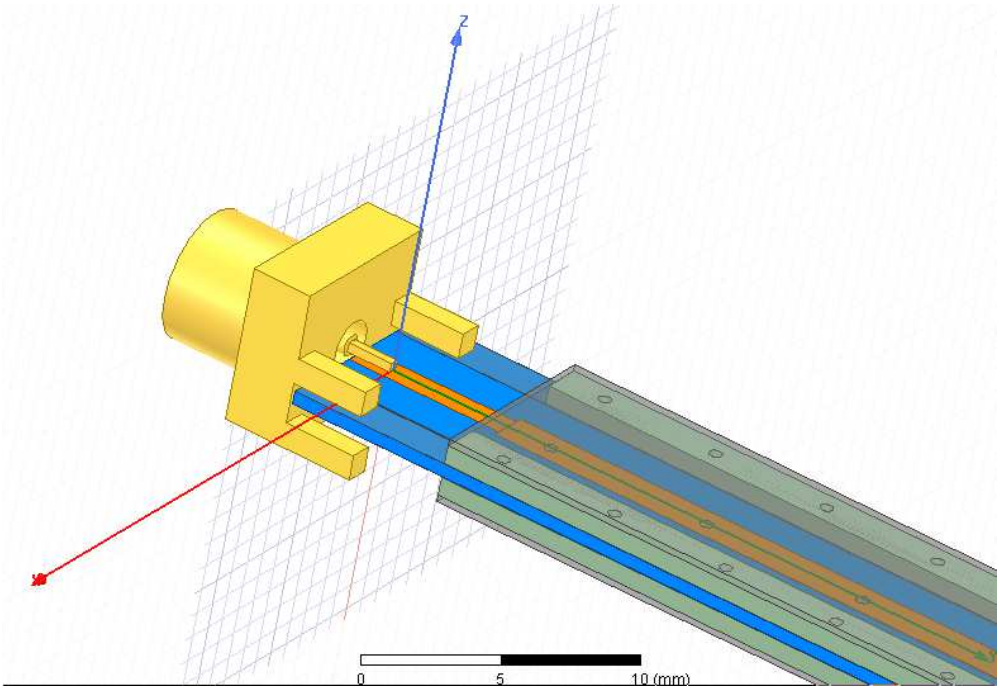

Figure 49 – SMA to MLIN to DSSL Transition in HFSS

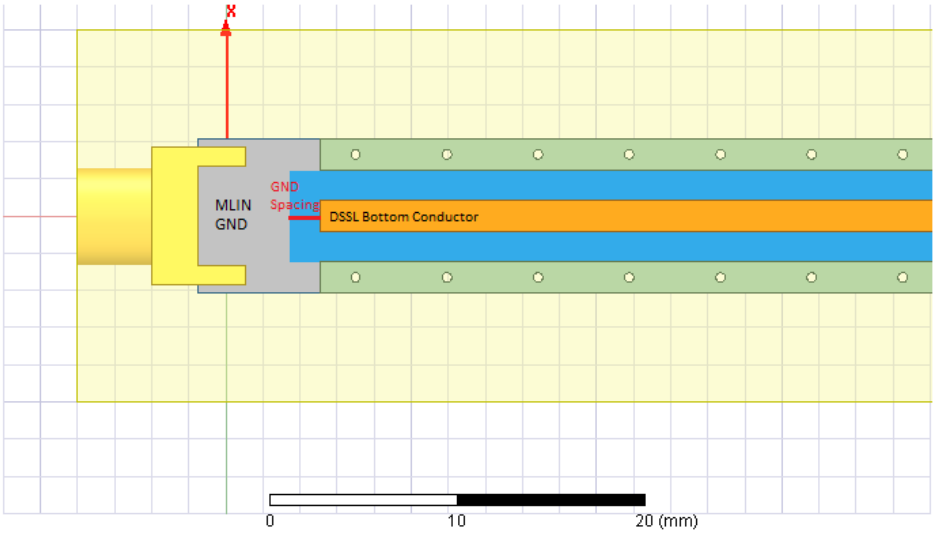

Figure 50 – Bottom View of the Transition with Ground Spacing Between MLIN and DSSL

Figure 49 shows the entire SMA to microstrip to DSSL transition in HFSS. Figure 50 shows a bottom view of the transition. The microstrip line needs a ground reference on the bottom of the substrate, but the bottom conductor of the DSSL is also on the bottom of the substrate. Obviously the microstrip ground cannot be connected to the bottom DSSL conductor otherwise the signal will be short circuited to ground. The spacing between the microstrip ground reference and the DSSL bottom conductor was a parameter optimized in HFSS. This optimal ground spacing was found to be 105mils, which is roughly 1.5 line widths.

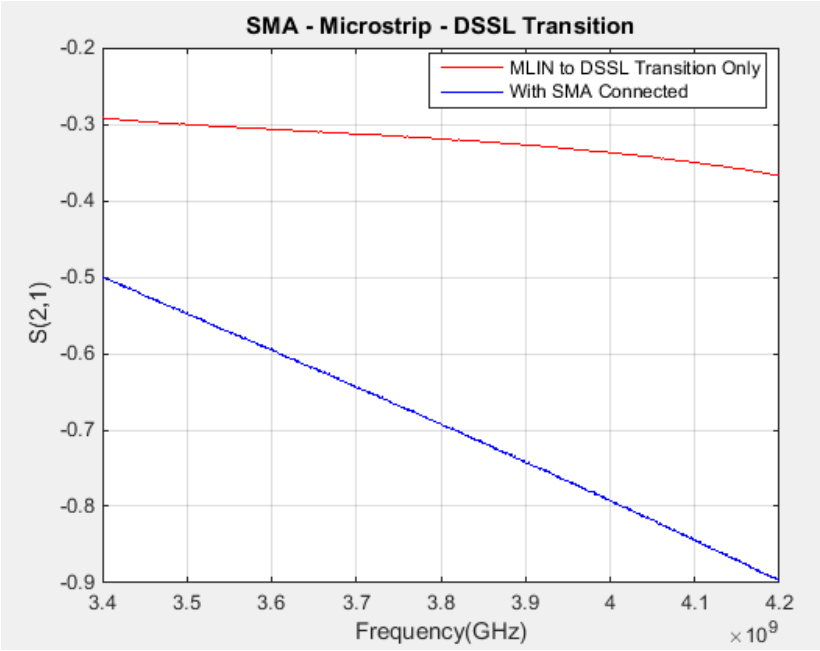

Figure 51 – Transition Response with and without SMA Connected

Figure 51 shows the transmission response of an microstrip to DSSL transition with and without the SMA. The microstrip to DSSL transition adds about 0.2dB of loss when compared with a thru DSSL, and the SMA adds an additional 0.4dB of loss at the center frequency. These results are reasonable and

show that a low loss SMA to microstrip to DSSL transition can be designed using HFSS.

4 CONCLUSIONS AND FUTURE WORK

Design Process

The design process starts by defining the substrate material and the substrate thickness. After the material definitions are set, ADS Linecalc (or equivalent method) can be used to determine the optimal width of a *standard* suspended stripline. The following equation can then be used to produce an initial value for the width of a 50Ω DSSL from a standard suspended stripline:

$$\left(\sqrt{\frac{\varepsilon_{e_{SSL}}-1}{\varepsilon_{r_{SSL}}+1}}\right) * \left(W_{SSL}(mm)\right) + 0.968 = W_{double}(mm)$$

The equation is a very good approximation for the optimal width of DSSL, but further optimization should be done to find the precise width required for 50Ω line. This equation was empirically derived through many simulation results and was applied to many different design examples. In each case, the equation does yield a reasonable approximation for the optimal width of a given DSSL design. Once the optimal width is found, the physical dimensions of the DSSL structure can be assigned.

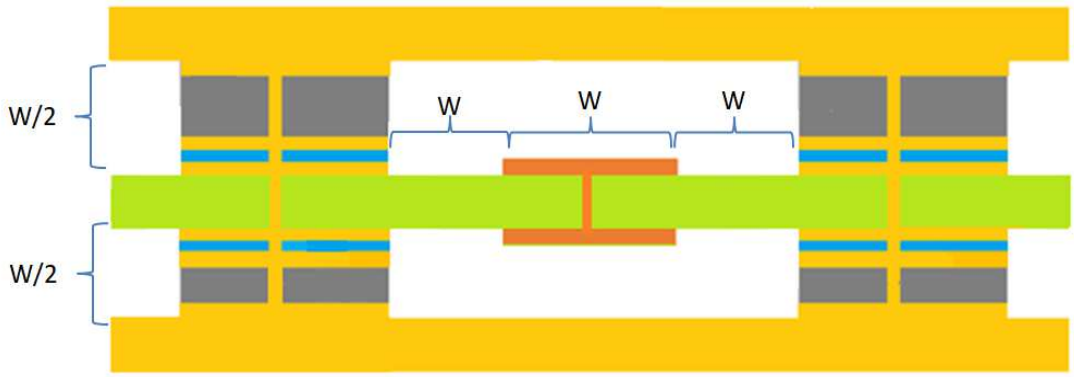

Figure 52 – Dimensions for DSSL

There should be at least one line width spacing on either side of the signal trace. The air gap spacing above and below the board should be approximately equal to one-half of the line width. Further optimization should be performed to determine the ideal air gap spacing.

Other parameters such as guided wavelength and effective permittivity can be easily determined in simulation by adjusting the length of the DSSL until a 360 degree phase is achieved. The relation $(\frac{\lambda_0}{\lambda_g})^2 = \varepsilon_e$ can then be used to determine the effective permittivity of a given design.

Future Work

This thesis describes some initial research that has been done into the merits and implementation of DSSL transmission media design. In this section, some future directions for research will be expanded upon. This thesis has expanded on previous work by laying out some general guidelines and observations of DSSL and how it compares to other transmission media. This thesis has also successfully applied a DSSL design to a

planar orthomode transducer circuit, proving that in some instances this design can be quite feasible—in terms of both performance and price. Future work should involve developing more empirical design equations and software models that can be used to design and implement DSSL structures.

Other future work could include developing passive microwave components in DSSL such as filters, power dividers, and couplers. Developing methods to integrate surface mount components and lumped elements into a DSSL design could also be hugely insightful and expand the instances in which DSSL could be used.

REFERENCES

[1] Y. Toeda, T. Fujimaki, M. Hamada, T. Kuroda, "Fully integrated OOK-powered pad-less deep sub-wavelength-sized 5-GHz RFID with on-chip antenna using adiabatic logic in 0.18μm CMOS", in 2018 Symposium on VLSI Circuits Digest of Technical Papers, pp. 27-28, Keio University, Yokohama, Kanagawa, Japan. 2018.

[2] X. Mi, T. Takahasi, S. Ueda, "Integrated Passives on LTCC for Achieving Chip-Sized-Modules", Proceedings of the 38th European Microwave Conference, pp. 607-610, Fujitsu Laboratories Ltd. 64, Nishiwaki, Ohkubo-cho, Akashi 674-8555, Japan, October 8, 2008. Accessed February 3, 2019.

[3] U. Singh, M. Green, "High-Frequency CML Clock Dividers in 0.13- μm CMOS Operating Up to 38 GHz", IEE Journal of Solid-State Circuits, Vol. 40, No. 8, pp. 1658–1660, August 2005. Accessed February 3, 2019.

[4] E. Sandhiya, D. Denis, I. C. Hunter, "Novel Design Methodology for High Efficiency Class E Microwave Frequency Triplers", pp. 1825-1828, Institute of Microwaves and Photonics, School of Electronic and Electrical Engineering, University of Leeds, Leeds LS2 9JT, UK., 2006. Accessed February 3, 2019.

[5] Y. Tian, H. Wang, Z. Liu, Q. Meng, K. Lee, "Low-Loss Microcoaxial Rat-Race Hybrid for Si-Based Microwave Integrated Circuits", IEEE Microwave and Wireless Components Letters, VOL. 26, NO. 3, pp. 162-164, March 2016, Accessed February 3, 2019.

[6] X. Liu, Z. Zhu, Y. Yang, R. Ding, "Low-Loss Air-Cavity Through-Silicon Vias (TSVs) for High Speed Three-Dimensional Integrated Circuits (3-D ICs)", IEEE Microwave and Wireless Components Letters, VOL. 26, NO. 2, pp. 89-91, February 2016, Accessed February 3, 2019.

[7] Casini, E., Gallinaro, G., Grotz, J., "Reduced front-end reception requirements for satellite broadcast using interference processing", *IEEE Transactions on Consumer Electronics*, VOL 54, NO. 4, pp.1555-1563, August 21, 2008. Accessed February 3, 2019

[8] D. M. Pozar, "Transmission Lines and Waveguides", in Microwave Engineering, 4th ed., Hoboken, NJ, USA, John Wiley & Sons Inc., 2012, ch. 3, sec. 3.7-3.8, pp. 141-147.

[9] Na.support.keysight.com," *Analyzing Transmission Line Parameters"*. ,2019, online, available at: http://na.support.keysight.com/plts/help/WebHelp/Analyzing/Analyzing_Transmission_Line_Parameters.html Accessed 3 Feb. 2019.

[10] Li, L., Ma, K., Mou, S. (2017). "A Novel High Q Inductor Based on Double-sided Substrate Integrated Suspended Line Technology with Patterned Substrate", 2017, School of Physical Electronics, University of Electronic Science and Technology of China, Chengdu, China. Accessed February 3, 2019.

[11] Xia, L., Song, L., Wu, B., Bo, X., Chen, J., "Double-layer suspended stripline resonator with high quality factor for base-station diplexer application". Electronics Letters, Vol. 54, NO. 8, pp. 513-515, April 19, 2018. Accessed February 3, 2019.

[12] Chen, J., Chin, C. and Xue, Q., "Double-Sided Parallel-Strip Line With an Inserted Conductor Plane and Its Applications". *IEEE Transactions on Microwave Theory and Techniques*, VOL 55, NO. 9 , pp.1899-1904, September 2007. Accessed February 3, 2019.

[13] Rogerscorp.com, "RO400 Laminates: RO4003C and RO4350B – Data Sheet", 2019, online, available at http://www.rogerscorp.com/documents/726/acs/RO4000-Laminates-RO4003C-and-RO4350BData-Sheet.pdf. Accessed February 19, 2019.

[14] Rogerscorp.com, "RT/duroid 5870/5880 – Data Sheet", 2019, online, available at http://www.rogerscorp.com/documents/606/acs/RT-duroid-5870-5880-Data-Sheet.pdf Accessed February 19, 2019.

[15] D. M. Pozar, "Power Dividers and Directional Couplers", in Microwave Engineering, 4th ed., Hoboken, NJ, USA, John Wiley & Sons Inc., 2012, ch. 7, sec. 7.8, pp. 363-364

[16] Saidimanesh, H., Ghorbanzade, P., "Design and Simulation of a Low-Cost X-Band Orthomode Transducer". 21st Telecommunications forum TELEFOR 2013, Serbia, Belgrade, November 26 – 28, 2013. Accessed March 2, 2019.

[17] Abdelaal, M., Shams, S., Kishk, A., "Asymmetric Compact OMT for X-Band SAR Applications", Transactions on Microwave Theory and Techniques, Vol. 66, NO. 4, pp.1856 – 1863, April 2018. Accessed March 2, 2019.

[18] sagemillimeter.com, "8.2 to 12.4 GHz, 30 dB Isolation, 35 dB Cross Polarization, 0.900" x 0.900" Square Waveguide Antenna Port, X Band Orthomode Transducer", online, available at: https://www.sagemillimeter.com/8-2-to-12-4-ghz-30-db-isolation-35-db-cross-polarization-0-900-x-0-900-square-waveguide-antenna-port-x-band-orthomode-transducer/. Accessed March 27, 2019.

[19] Digikey.com, "Amphenol RF SMA Connector Products", online, available at, "https://www.amphenolrf.com/media/downloads/1848/132357-11.pdf". Accessed February 26, 2019.